UNIVERSIDADE DE SÃO PAULO
INSTITUTO DE FÍSICA DE SÃO CARLOS

Edward Gutenberg Iraita Salcedo

The gray molasses cooling technique for optimizing the temperature of 39K atoms

São Carlos

2021

Edward Gutenberg Iraita Salcedo

The gray molasses cooling technique for optimizing the temperature of 39K atoms

Dissertation presented to the Graduate Program in Physics at the Instituto de Física de São Carlos, Universidade de São Paulo, to obtain the degree of Master of Science.

Concentration area: Basic Physics

Advisor: Prof. Dr. Vanderlei Salvador Bagnato

Corrected version

(Original version available on the Program Unit)

São Carlos

2021

Iraita Salcedo, Edward Gutenberg
The gray molasses cooling technique for optimizing the temperature of 39K atoms / Edward Gutenberg Iraita Salcedo; advisor Vanderlei Salvador Bagnato - corrected version -- São Carlos 2021.
84 p.

Dissertation (Master's degree - Graduate Program in Basic Physics) -- Instituto de Física de São Carlos, Universidade de São Paulo - Brasil , 2021.

1. Bose-Einstein condensate. 2. Optical molasses. 3. Gray molasses. 4. Magneto optical trap. I. Bagnato, Vanderlei Salvador, advisor. II. Title.

ACKNOWLEDGEMENTS

En primer lugar quisiera agradecer a Dios por estar siempre a mi lado, por cuidar a mi linda familia que no la tuve cerca durante este trabajo, pero si presente con toda la fuerza del corazon, pues a ellos les dedico mi trabajo, por sus lindas palabras y risas durante las llamadas telefonicas, a mi chinita Helen, a mi Marita, a mi sobrinito Derick, a mi Mamita Luisa y a mi Papito Gerardo, esto es por ustedes familia preciosa, siempre unidos. Y tambien a mis hermosas amistades que me puso la vida. Y como no agradecer a todos los trabajadores de la salud, de la seguridad y de la salubridad, que estuvieron expuesto a ese enemigo inivisible. Este trabajo fue alcanzado con toda la ayuda de Kilvia, Emmanuel, Paty, Pedro, Arnol, Leandro y al profesor Vanderlei Bagnato por mostrarme y ofrecerme su apoyo en todo momento. A estas maravillosas personas, les digo muchas gracias con lo mas profundo de mi corazón.

It takes a moment to tell someone you love them,

but it takes a lifetime to prove it

- Erich Fromm

ABSTRACT

IRAITA SALCEDO, E. G. **The gray molasses cooling technique for optimizing the temperature of 39K atoms**. 2021. 84p. Dissertation (Master in Science)-Instituto de Física de São Carlos, Universidade de São PauloInstituto de Física de São Carlos, Universidade de São Paulo, São Carlos, 2021.

Alkali-metal atoms are the foremost candidates for studies of degenerate quantum gases employing sub-Doppler cooling techniques operating either on the D1 or D2 transition. However, the case of ^{39}K atoms has a narrow excited-state structure of the D2 transition compromising difficulty to achieve below the Doppler limit temperature ($T_D = \hbar\Gamma/2k_B = 140\mu K$) by employing conventional cooling techniques such as optical molasses or polarization gradient cooling on this transition. In this work, a sub-Doppler cooling known as Gray molasses operating on the $|4^2S_{1/2}\rangle \rightarrow |4^2P_{1/2}\rangle$ 770nm transition D1 is applied to cool a cloud of ^{39}K atoms to sub-Doppler temperatures, which is an important step to reach the quantum degeneracy of the quantum gases. With this approach we reach temperatures below the Doppler limit around 14.3μK by the formation of dark states using the cooling and repumping lasers detuned to the blue side at the Raman resonance (two-photon) in Λ configuration. Then, we ramp down the intensities of each laser beam, in order to cool the atoms to an ultra-low temperature of 8.62μK, getting closer to the photon recoil limit of ($T_r = \hbar^2k_L^2/2mk_B = 0.4\mu K$). In our results, we present a study of the behaviour of the temperature and the number of atoms by the influence of the relative detuning, and also a particular analysis of the temperature by the influence of the global detuning. In the following, we present the lowest temperature as a function of the final intensities D1 molasses. Finally, we compare the performance of our Gray molasses cloud with other works by using a phase space density analysis.

Keywords: Bose-Einstein condensate. Optical molasses. Gray molasses. Magneto optical trap.

RESUMO

IRAITA SALCEDO, E. G. **Técnica de resfriamento molasses cinza para a otimizaçãon de temperatura do 39K**. 2021. 84p. Dissertação (Mestrado em Ciências) - Instituto de Física de São Carlos, Universidade de São PauloInstituto de Física de São Carlos, Universidade de São Paulo, São Carlos, 2021.

Átomos alcalinos são fortes candidatos para experimentos para estudos em gases quânticos degenerados, uma vez que empreguemos técnicas de resfriamento sub-Doppler, tanto operando na transição D1 ou D2. Entretanto, átomos de ^{39}K tem uma estrutura de estado excitado estreita, o que compremete alcançar temperaturas abaixo do limite Doppler, usando a transição D2 ($T_D = \hbar/\Gamma/2k_B = 140\mu$K), empregando técnicas convencionais de resfriamento, como molasses óptico ou resfriamento por gradiente de polarização. No presente trabalho, um tipo de resfriamento sub-Doppler conhecido como Gray molasses, o qual opera na transição D1 $|4^2S_{1/2}\rangle \rightarrow |4^2P_{1/2}\rangle$ 770nm, é aplicada para resfriar uma nuvem de átomos de ^{39}K a temperaturas sub-Doppler. Este é um importante passo para alcançar a degenerescência quântica e, em nosso caso, obtivemos temperaturas abaixo do limite Doppler em torno de 14.3μK. Isso é possível pela formação de estados escuros usando lasers de resfriamento e de rebombeio, dessintonizados para o azul da ressonância Raman (dois fótons) em configuração λ. Em seguida, fizemos uma diminuição controlada, em uma rampa, das intensidades de cada feixe laser. Dessa forma, resfriamos os átomos a uma temperatura muito baixa como 8.65μK, a qual está próxima à temperatura limite de recuo ($T_r = \hbar^2k_L^2/2mk_B = 0.4\mu K$). Em nossos resultados, apresentamos um estudo do comportamento da temperatura e número de átomos pela influência da dissintonia relativa de frequências, e também uma análise particular da temperatura pela influência da dessintonia global. Em seguida, apresentamos a temperatura mais baixa como função das intensidades finais de molasses. Finalmente, comparamos a performance de nossa Gray Molasses com outros trabalhos usando uma análise por densidade no espaço de fase.

Palavras-chave: Condensado de Bose-Eisntein. Melaza óptica. Melaza cinza. Armadilha magneto óptica.

LIST OF FIGURES

Figure 1 – Optical molasses scheme in one dimension for a two level atom that has a velocity component v along the z-axis. 32

Figure 2 – Mechanism of the MOT in one dimension for two level atom with resonance frequency ω_0 corresponding to the transition $J = 0 \rightarrow J = 1$. Spatial Zeeman splitting of the exited state provides a confinement for atoms in the zeropoint at the center. The frequency ω of the two counter propagating laser beams is red detuned by Δ from resonance. The length of the black arrows represents the strength of the quadrupole magnetic field. 35

Figure 3 – Magneto optical trap in an anti-Helmholtz configuration, described in a transition $J = 0, 1$. The white arrows indicate the current direction for each coil. In the plane xy, the polarization of the light is σ^-, whereas for the z-axis, the polarization of the light is σ^+. 36

Figure 4 – Schematic of Sisyphus cooling for $J_g = 1/2 \rightarrow J_e = 3/2$ transition in Lin $\perp$ Lin configuration. The upper portion shows the polarization set up by the two beams. The lower figure shows the ground state sublevels which are light shifted by the polarization gradient set up. 37

Figure 5 – Trivial dark states for σ^+ and σ^- polarized light for a $F = 2 \rightarrow F' = 2$ optical transition. 42

Figure 6 – Magnetic sublevels for a $J_g = 1 \rightarrow J_e = 1$ transition. The atomic states are labeled using two quantum numbers : magnetic quantum number that specifies the internal spin and the z component of the external momentum. 43

Figure 7 – Transitions strengths for a ^{39}K atoms for σ^+ polarization. The hyperfine states of the (D1) transition from $4^2S_{1/2}$ to $4^2P_{1/2}$ are illustrated. . . . 45

Figure 8 – Transitions strengths for ^{39}K atoms for σ^+ polarization. The hyperfine states of the (D2) transition from $4^2S_{1/2}$ to $4^2P_{3/2}$ are illustrated. . . . 45

Figure 9 – Atoms in Gray molasses scheme. Three counter-propagating beams covering all three directions. The atoms (green) are located in the center of the intersection. 46

Figure 10 – Working scheme of the Gray molasses cooling technique for different detunings. 47
Figure 11 – A three level Λ-system of two ground states $F = 1$ and $F = 2$ of $^2S_{1/2}$ and the excited state $F' = 2$ of $^2P_{1/2}$ of ^{39}K. The repumping beam of frequency ω_1 and detuning δ_1 couples the $F = 1 \rightarrow F' = 2$ transition, whereas the cooling beam of frequency ω_2 and detuning of δ_2 couples the $F = 2 \rightarrow F' = 2$ transition. 48
Figure 12 – D1 and D2 transition laser cooling beam detunings. 50
Figure 13 – The magnetic sublevel states of ^{39}K (D1) transition with the allowed transitions depending on the polarization in Gray molasses. Trivial dark states are marked with blue circles and the additional non-coupled states are marked by red elipses. 51
Figure 14 – Optical table where the vacuum system is installled. 53
Figure 15 – Vacuum system made up of sections: The first one on the left side shows one of the chambers (HVS) for the 2D-MOT K process. In the center, the chamber (UHV) or science chamber is shown. The last one on the right side shows one of the cameras (HVS) for the 2D-MOT Na process. 54
Figure 16 – On the top of Science Chamber we have the upper coil of quadrupole field. 54
Figure 17 – Laser system for the generation D2 beams. 56
Figure 18 – Laser system for the generation D1 beams. 57
Figure 19 – Illustration of the configuration of the image table. There we can choose between two magnifications to observe our cloud of atoms in the horizontal plane x-y. 59
Figure 20 – Experimental sequence with the magnetic field and light of each step. . 60
Figure 21 – ^{39}K 3D-MOT loading as a function of time. The 3D-MOT loading rate proportional to the 2D-MOT atomic flux can be obtained by performing a linear adjust at the initial part of the 3D-MOT loading curve (red curve) for which we obtained $L = 1.33 \times 10^7$ atoms/s, being L the atomic flux. 61
Figure 22 – (a) The red cloud shows the fluorescence of potassium atoms in the science chamber. (b) Image of the ^{39}K 3D-MOT, captured with a CCD camera Allied Vision model Stingray F-145. 62

Figure 23 – Hybrid C-MOT. Left: The atomic cloud without compressed MOT.Right: The atomic cloud with compressed MOT. 62
Figure 24 – Sequence image for 39K. 63
Figure 25 – Imaging processing to obtain the normalized absorption image of the atoms after the Gray molasses stage. 64
Figure 26 – The time of flight technique for two times of flight t_1 and t_2. 65
Figure 27 – The time of flight technique for different times of flight between 10ms and 17ms. The blue and red slope represent the temperature by fitting equation 5.6 for x and y dimension respectively. 66
Figure 28 – Level scheme of the transitions used for D1 Gray molasses cooling for 39K working on the $F = 2 \rightarrow F' = 2$ transition. 69
Figure 29 – Temperature as a function of duration in Gray molasses. 70
Figure 30 – Number of atoms as a function of duration in Gray molasses. 71
Figure 31 – Temperature of the (D1) Gray molasses as a function of Raman detuning d. Deep cooling is found at the Raman resonance. The cooling at 14.3 μK observed on both sides of the resonance is attributed to the Gray molasses mechanism working on the $F = 2 \rightarrow F' = 2$ transition. 72
Figure 32 – Number of atoms in Gray molasses as a function of Raman detuning d. 73
Figure 33 – Temperature of the (D1) gray molasses as a function of the global detuning Δ of the D1 cooling beams. 74
Figure 34 – Two-stage cooling scheme. A capture phase and constant cooling power at 114 I_s with a duration of 1 ms is followed by a cooling phase of 4ms in which the intensity is ramped down to 0.28 I_s of the initial cooling intensity. 75
Figure 35 – Temperature of Gray molasses vs total power (D1) light beam. 76
Figure 36 – Number of atoms, temperature and the phase space density fo some works related to precooling potassium atoms. NR: Not realized, NS: Not specified. 77

LIST OF ABBREVIATIONS AND ACRONYMS

AOM	Acoustic-Optical Modulator
BEC	Bose-Einstein Condensate
CMOT	Compressed Magneto-Optical Trap
GM	Gray Molasses
MOPA	Master Oscillator Power Amplifier
MOT	Magneto-Optical Trap
MT	Magnetic Trap
ODT	Optical Dipole Trap
SC	Science Chamber
VCO	Voltage-Controlled Oscillator

CONTENTS

1 INTRODUCTION 19

2 LASER COOLING AND TRAPPING 23

2.1 Semi-classical theory for cooling in a two-level atomic system 24

2.2 Light forces 25

2.3 Doppler cooling and optical molasses 30

2.4 Magneto optical trap 34

2.5 Cooling beyond the Doppler limit: sub-Doppler cooling 36

2.5.1 Sisyphus cooling: lin-perp-lin (1-D model) 37

2.5.2 Corkscrew cooling: σ^+-σ^- (1-D model) 39

2.5.3 Recoil limit 40

3 THE GRAY MOLASSES COOLING TECHNIQUE 41

3.1 Trivial dark states 41

3.2 Non-coupled states $|\Psi_{NC}\rangle$ and velocity-selective coherent population trapping (VSCPT) 42

3.3 D1 transition 44

3.4 Principle of Gray molasses 45

3.5 Λ configuration and coherent dark state 46

3.6 Cooling scheme of the Gray molasses on the D1 transition of ^{39}K . 50

3.7 Raman-resonance condition 51

4 EXPERIMENTAL SETUP 53

4.1 The vacuum system 53

4.2 Optical system 55

4.2.1 Lasers on D2 line 55

4.2.2 Lasers on D1 line 57

4.3 The absorption image technique 58

4.4 Time sequence of the experiment 60

4.4.1 Loading of magneto optical trap 60

4.4.2 Imaging procedure for ^{39}K 63

4.5 Measurement of temperature and number of atoms in gray molasses 64

5 RESULTS AND DISCUSSION 69

5.1 Characterization of Gray molasses 69

5.1.1 Gray molasses timings 70

5.1.2 Raman detuning 71

5.1.3 Light Intensity 75

5.2 Phase space density analisys 76

6 CONCLUSIONS AND PROSPECTS 79

REFERENCES 81

1 INTRODUCTION

The Bose-Einstein condensation (BEC, from the english Bose-Einstein Condensation) occurs when, below a critical temperature, the particles of a bosonic system collectively occupy the state of lower energy.[1−2] At these low temperatures, the thermal de Broglie wavelength of each atom will become comparable to interatomic separation such that the atoms become indistinguishable and their individual wave functions overlap to form a collective macroscopic wave function.[3] That macro-occupation in a single state that makes the condensates exhibit strictly quantum properties. This type of system becomes interesting once it is fully governed by the laws of quantum mechanics[4] and also for presenting macroscopic quantum effects[5−6] for allowing the simulation of other diverse quantum systems, with special emphasis on solid-state physics.[7−8] In addition to producing technological advances[9] or as to also extend the production of such a phase for exotic gases.[10]

The research center (CePOF) coordinated by Professor Vanderlei S. Bagnato has been working with cold atom systems and some years ago it was the first group to produce BEC in Latin America.[11] In recent years, the group conducted a series of studies of vortices and superfluids, exciting the condensate with a temporarily oscillating magnetic field. In this context, an out-of-phase oscillation between the condensate and the thermal cloud was observed,[12] vortex nucleation,[13] and the first evidence of quantum turbulence in dilute gas condensate.[14] The possibility of producing ultra-cold gases with different atomic species introduces a richer scenario to study vortices and quantum turbulence. Currently, one of the great interests of our research group is to study these phenomena in a system of two ultra-cold atomic species, sodium (^{23}Na) and potassium (^{39}K or ^{41}K).

Experimental studies of Bose Einstein condensation require various stages, most of which involve optimizing the cooling processes of the atomic sample. In this dissertation, we will discuss one of the most important cooling steps for the potassium-39 atoms, decreasing its temperature and increasing the phase space density. As the first stage, the vapor of the potassium atoms will be carried out in a 2D magnetic-optical trap (2D-MOT)[15−16] , where the Doppler cooling will take place, then they are transferred and recaptured in a 3D magnetic-optical trap (3D-MOT). After these stages they will go to conservative traps,

being either magnetic trap (MT) or optical dipole trap (ODT).

One of the main objectives in our laboratory is the formation of the mixture of the condensates of both species ^{23}Na and ^{39}K, however to cool the sample of ^{39}K, we will use the process of sympathetic cooling,[17] where the atomic sample of ^{23}Na act as a cold machine (refrigerant) and the atomic sample of potassium act as a the warm machine and through collisions between these species reach thermal equilibrium. Because the atomic sample of potassium are hotter than the atomic sample of sodium. Therefore, ^{39}K will heat the sodium atomic sample, that is why we need to cool the atomic potassium sample to get the least increase in temperature for the atomic sodium sample.

To cool the cloud of atoms it is necessary to find a way to reduce the entropy of the gas. Optical molasses is a cooling technique that uses momentum transfer between photons and atoms reducing the speed of distribution of the atomic cloud that is, spontaneous emission is the mechanism where Doppler cooling dissipates energy from the atomic cloud. However, this mechanism will have a limit due to the stochastic nature, it is that the atoms go towards different directions, which will heat up the neighboring atoms through spontaneous emission, which is the limit of this mechanism for ^{39}K this limit is called the Doppler temperature and will be 146μK.

To go beyond this cooling limit, we will use another sub-Doppler cooling technique called Gray molasses, which involves three theoretical concepts: the existence of dark states, the Sysiphus cooling mechanism, and the lambda configuration. This technique was used in atoms of sodium, cesium, rubidium, but in the D2 line of their hyperfine structure. However, for ^{39}K its small hyperfine structure on the D2 transition makes it very difficult to cool. One of the first problems with cooling potassium 39 is its small background scattering length, which will give a less effective evaporation process. The background interaction strength is attractive for ^{39}K, which will give us an instability in the condensate (BEC) which we will solve by entering the D1 line with the Gray molasses.

The Gray molasses cooling technique was proposed in the references[18−19] and the first experimental realizations were in the samples of ^{133}Cs[20−21] and ^{87}Rb,[22] and more recently in ^{40}K,[23] ^{87}Rb[24] and ^{23}Na,[25] using the transitions on the D2 transition line. Nowadays, this same technique is widely used to cool atoms more efficiently by applying light at D1 line transition. Furthermore, the D1 line where Gray molasses will

take place, the Rabi frequencies for each transition between $|F = 2\rangle \rightarrow |F' = 2\rangle$ transition is proportional to their Clebsch-Gordan cofficientes and these cofficients are less than the ones for D2 line. Then, their Rabi frequencies will be proprtional to the temperature by the equipartition theorem.

In Chapter 2, we make an introduction to the theory of laser cooling and trapping in one dimension and for a two level atom system using a semiclassical picture for the atomic interaction with light field. In Chapter 3 are revised the basic concepts of the Gray molasses cooling technique. In Chapter 4, we will detail the experimental apparatus, where different cooling and capture techniques are carried out. And finally, in Chapter 5, also we present a PSD analysis comparing our result with other experiments. In Chapter 6, the results concerning the Gray molasses cooling technique are present and their respective discussion for each result.

2 LASER COOLING AND TRAPPING

The theory of laser cooling and trapping has revolutionised many exciting experiments in atomic physics field. The light as radiation pressure was proposed by Hansch and Schawlow for gas of neutral atoms in 1975, who demonstrated that the Doppler effect provides a velocity dependent force when illuminating neutral atoms with laser radiation. This theory was carried out experimentally by Chu et al. in 1985, who demostrated the effect of the Doppler cooling in three dimensions to obtain very cold atoms. That work introduced the so-called optical molasses. However, optical molasses cannot trap atoms due to the momentum diffusion of the atoms. Latter this paved the way to develop the so-called Magneto Optical Trap (MOT) which was reporter in 1987 by Raab et al, though the seminal idea is credited in that paper to Jean Dalibard. This confinement technique is considered as the backbone in most cooling and trapping experiments. Today, laser cooling and trapping are standard techniques for all experiments investigating quantum degenerate gases. The interaction between atom and light allow us to cool atomic samples at temperatures in the micro and nanokelvin range by the use of energy and momentum conservation. This chapter will summarize the theorical basics of laser cooling and trapping such as light forces, optical molasses, magneto optical trap and sub-Doppler cooling techniques which are necessary to understand the working principles of the employed techniques.

There are three processes that constitute all of the atom-light interactions: spontaneous emission, absorption and stimulated emission of photons. The force exerted on the atoms by the laser radiation can be divided into two components: the radiation pressure force, or dissipative force, which is based as a result of absorption and spontaneous emission of photons causing the slowing and then cooling of the atoms and will allow us to understand the "optical molasses" cooling technique. The second component is the dipole force, or the gradient force, which is based as a result of cyclical processes of absorption and stimulated emission of photons. This dipole force is proportional to the field gradient. The atomic cloud will be considered a well diluted atomic medium, that is, we can ignore the atom-atom interaction.

2.1 Semi-classical theory for cooling in a two-level atomic system

As we know, real atoms can have many degenerate states of energy, they also present movement, collide with each other, and are subject to spontaneous emission. The electromagnetic fields that interact with atoms can contain different plane wave modes. Due to all these factors, the theoretical study becomes complex, for this reason, is necessary to separate several physical regimes.

Therefore, the development to be taken into account in this section will be of a semiclassical treatment, which implies two fundamental assumptions. The first assumption is that the center of mass of the atom is described by a small wave packet, i.e. $\Delta x << \lambda$ where Δx it is the uncertainty of the atom's position and λ is the wavelength of light field (Laser). The second assumption is that the velocity of the atom must be well defined so that the uncertainty in the atomic Doppler shift must be less than the atomic transition linewidth. That is, $k\Delta v << \Gamma$, where k is the light wavenumber $k = 2\pi/\lambda$, Δv is the velocity spreading of the atomic wavepacket, and Γ is the natural linewidth of the atomic transition.

In this semiclassical treatment, the atom can be seen as a (positive) center immersed in a cloud of (negative) electronic charge, whose spatial distribution depends on the energy state of the system. When the electromagnetic radiation (Laser) interacts with the charge distribution and there will be a relative displacement of the negative and positive charges resulting in an induction of multipolar moments.

Therefore, the simplest interaction that occurs between the atom and the electromagnetic field is an electrical dipole type interaction. If we call $\vec{\mu}$ the electric dipole moment induced in the atom by electromagnetic radiation, the energy of this interaction is given by:

$$H_{int} = -\vec{\mu}.\vec{E} \tag{2.1}$$

Where

$$\vec{\mu} = -e.\vec{r} \tag{2.2}$$

In this interaction, the electromagnetic radiation produces a distribution of charges in the atom, in that way that the system presents an electric dipole. This interaction, called the electric dipole approximation, is undoubtedly one of the most important and therefore we will take it as predominant when treating the atomic system on two levels.

Suppose that an atom consists of two levels, escapes a lot from reality, since the simplest atom is far from having two levels, but it happens to be reasonable when the light field is near resonance with an atomic transition. Thus the two levels involved in the transition are singled out by the laser frequency and polarisation.

2.2 Light forces

In the previous treatment only made a brief study of the energy change between the atomic system and radiation. However there is also another type of effect in this interaction, that is, due to the energy transfer there will also be momentum transfer, therefore the atomic system will be subject to a force with which we can control the external degrees of freedom, for instace, the movement of the atom. This force will have the name of radiative force, which we will see later that this force will be composed of two forces.

To obtain these forces, we will make a more general treatment including a unified treatment of the radiation force including the effects of spontaneous emission and the induction of the dipole interaction, and the Hamiltonian is considered an additional term due to the movement of the center of mass. Using Ehrenfest's theorem and Bloch's optical equations, taking into account that the atomic motion will interact with resonant wave or near to resonance.[26]

In a classical electromagnetic wave, and using dipole approximation.The Hamiltonian for an atom is:

$$H = \frac{\vec{P}^2}{2m} + H_o - \vec{\mu}.\vec{E}(\vec{R},t) \tag{2.3}$$

The first term represents the kinetic energy associated with the center of mass, H_o is the Hamiltonian for the internal motion for the unperturbed atom, $\vec{\mu}$ is the electric dipole operator, $\vec{E}(\vec{R},t)$ is the electric field at the center of mass position $\vec{R}$ whose coupling $\vec{mu}$ is the interaction of the atom with radiation.

In the Heisenberg representation, the operators $\vec{R}$ and $\vec{P}$ satisfy equations of motion:

$$\dot{\vec{R}} = \frac{i}{\hbar}[H, \vec{R}] = \frac{1}{i\hbar}[\vec{R}, H] = \nabla_p H = \vec{P}/M \tag{2.4}$$

$$\dot{\vec{P}} = \frac{1}{i\hbar}[\vec{P}, H] = -\nabla_R H = \nabla_R(\vec{\mu}.\vec{E}) \tag{2.5}$$

Then we can combine the expectations values (2.4) and (2.5), and setting $\vec{r} = \langle\vec{R}\rangle$. Now we can obtain Ehrenfest's theorem:

$$\vec{F} = m\ddot{\vec{r}} = \langle\dot{\vec{P}}\rangle = \langle\nabla(\vec{\mu}.\vec{E})\rangle \tag{2.6}$$

Considering an electric field of the form:

$\vec{E}(\vec{r}, t) = \hat{\epsilon}E(\vec{r}, t)$, with polarization vector $\hat{\epsilon}$ independent of $\vec{r}, t : \Rightarrow \vec{F} = \langle\vec{\mu}.\hat{\epsilon}\nabla E\rangle$, since ∇E is nearly uniform across the atomic wave packet:

$$\vec{F} = \langle\vec{\mu}.\hat{\epsilon}\rangle\nabla E(\vec{r}, t) \tag{2.7}$$

The internal motion of the atom is driven by the electric vector $\vec{E}(t) = \hat{\epsilon}E(\vec{r}, t)$, at the position of the moving atom and the Hamiltonian for the internal motion is $H' = H_o - \vec{\mu}.\vec{E}(t)$

Continuinig with the treatment of a two-level atomic system with energy levels E_1 and E_2 in an arbitrary monochromatic field.

$$E(\vec{r}, t) = \frac{1}{2}E(\vec{r})e^{i[\theta(\vec{r})+\omega t]} + c.c \tag{2.8}$$

With this radiation, the atomic system produce a mix of states:

$$\psi = C_1(t)\phi_1(\vec{r}) + C_2(t)\phi_2(\vec{r}) \tag{2.9}$$

Putting this wave function in the Schrödinger equation, and multiplying by ϕ_1^* and ϕ_2^* and

integrate respectively we have:

$$i\hbar\dot{C}_1 = E_1C_1 - \mu E(t)C_2$$

$$i\hbar\dot{C}_2 = E_2C_2 - \mu E(t)C_1 \tag{2.10}$$

Where $\mu = \langle 1|\vec{\mu}.\hat{\epsilon}|2\rangle$ is the transition dipole moment (here taken to be real), and $E(t) = E(\vec{r}(t), t)$, the general solutions of the two equations above is:

$$C_1 = D_1 e^{-i\frac{E_1}{\hbar}t + \frac{1}{2}i[\Delta t + \theta(\vec{r})]}$$

$$C_2 = D_2 e^{-i\frac{E_2}{\hbar}t - \frac{1}{2}i[\Delta t + \theta(\vec{r})]} \tag{2.11}$$

Where $\Delta = \omega - \omega_o(\omega_o = (E_2 - E_1)/\hbar)$ and the phase $\theta(t) = \theta(\vec{r}(t))$

From the equation of motion of C_1 and C_2 we get:

$$i\hbar\dot{D}_1 = \frac{1}{2}\hbar(\Delta + \dot{\theta})D_1 - \mu E(t)D_2 e^{-i(\theta+\omega t)}$$

$$i\hbar\dot{D}_2 = -\frac{1}{2}\hbar(\Delta + \dot{\theta})D_2 - \mu E(t)D_1 e^{i(\theta+\omega t)} \tag{2.12}$$

The we can insert (2.8) into equations (2.12) and neglecting terms that ocillates at twice the optical frequency rotating wave approximation (RWA), equation (2.12) reduce to

$$i\hbar\dot{D}_1 = \frac{1}{2}\hbar(\Delta + \dot{\theta})D_1 - \frac{1}{2}\mu E(t)D_2$$

$$i\hbar\dot{D}_2 = -\frac{1}{2}\hbar(\Delta + \dot{\theta})D_2 - \frac{1}{2}\mu E(t)D_1 \tag{2.13}$$

Now we will use the notation of density matrix, where the elements of the matrix will be given by $\rho_{nm} = C_nC_m^*$.

$$\begin{bmatrix} \rho_{gg} & \rho_{ge} \\ \rho_{eg} & \rho_{ee} \end{bmatrix} = \begin{bmatrix} \sigma_{gg} & \sigma_{ge}e^{i(\theta+\omega t)} \\ \sigma_{eg}e^{-i(\theta+\omega t)} & \sigma_{ee} \end{bmatrix} \tag{2.14}$$

Where $\sigma_{nm} = D_n D_m^*$ letting us to find the equations of motion (2.13) for σ_{nm}. In terms of those new elements of matrix:

$$\dot{\sigma_{11}} = \frac{-i}{2}(\Delta + \dot{\theta})\sigma_{11} + i\frac{1}{2\hbar}\mu E(t)\sigma_{21} + \frac{i}{2}(\Delta + \dot{\theta})\sigma_{11} - i\frac{1}{2\hbar}\mu E(t)\sigma_{12} \tag{2.15}$$

$$\dot{\sigma_{11}} = \dot{\sigma_{22}} = -\frac{1}{2}i\Omega(\sigma_{12} - \sigma_{21}) \tag{2.16}$$

$$\dot{\sigma_{12}} = -\frac{1}{2}i(\Delta + \dot{\theta})\sigma_{12} + \frac{1}{2\hbar}i\mu E(t)\sigma_{22} - \frac{1}{2}i(\Delta + \dot{\theta})\sigma_{21} - \frac{1}{2\hbar}i\mu E(t)\sigma_{11} \tag{2.17}$$

$$\dot{\sigma_{12}} = -i(\Delta + \dot{\theta})\sigma_{12} + \frac{1}{2}i\Omega(\sigma_{22} - \sigma_{11}) \tag{2.18}$$

Where $\Omega = \frac{\mu.E(t)}{\hbar}$ is the Rabi frequency for a two level atom in a field of amplitud $E(t)$.

Now the expectation value of the electrical dipole moment is:

$$\langle \vec{\mu}.\hat{\epsilon} \rangle = \int \psi \vec{\mu}.\hat{\epsilon}\psi d^3r = trace(\rho\mu) = \mu(\rho_{12} + \rho_{21})$$

$$\langle \vec{\mu}.\hat{\epsilon} \rangle = \mu[\sigma_{12}e^{i(\theta+\omega t)} + \sigma_{21}e^{-i(\theta+\omega t)}] \tag{2.19}$$

Of course, σ_{mm} are slowly varying function of time (these coefficient oscilate with Ω) when we compare with the optical frequencies ω (normally $\Omega \approx 10^6$Hz and $\omega \approx 10^4$ Hz).

Now recall that $\vec{F} = \langle \vec{\mu}.\hat{\epsilon} \rangle \nabla E(\vec{r}, t)$ and inserting into (2.19) and neglecting the

terms that oscillate at twice the optical frequency, we get:

$$\vec{F} = m\ddot{\vec{r}} = \frac{1}{2}\mu\nabla E(\sigma_{12} + \sigma_{21}) - \frac{1}{2}i\mu E\nabla\theta(\sigma_{12} - \sigma_{21}) \tag{2.20}$$

Now, we need to introduce relaxation terms in all calculation. The spontaneous emission will contribute as positive factor to $\dot{\sigma_{11}}$ and will be negative for $\dot{\sigma_{22}}$.

So, the spontaneuos emission is introduced in the calculations as follows:

$$\dot{\sigma_{11}} = -\frac{1}{2}i\Omega(\sigma_{12} - \sigma_{21}) + \Gamma\sigma_{22}$$

$$\dot{\sigma_{22}} = \frac{1}{2}i\Omega(\sigma_{12} - \sigma_{21}) - \Gamma\sigma_{22}$$

$$\dot{\sigma_{12}} = -\frac{1}{2}i(\Delta + \dot{\theta})\sigma_{12} + \frac{1}{2}i\Omega(\sigma_{22} - \sigma_{11}) - \frac{1}{2}\Gamma\sigma_{12} \tag{2.21}$$

Where $\Gamma = 4\omega_o^3|\langle 1|\vec{\mu}|2\rangle|^2/3\hbar c^3$ is the rate of spontaneous emission or also known as the coefficient A of Eisntein (the life time of the level is $\tau = 1/\Gamma$).

Let us define three new variables:

$$U = (\sigma_{12} + \sigma_{21}) \tag{2.22}$$

$$V = -i(\sigma_{12} - \sigma_{21})$$

$$W = (\sigma_{22} - \sigma_{11})$$

In terms of those new variables we have:

$$\vec{F} = m\ddot{\vec{r}} = \frac{1}{2}\hbar(U\nabla\Omega + V\Omega\nabla\theta) \tag{2.23}$$

And the equations that determine (U, V, W) are called Bloch's optical equations

$$\dot{U} = (\Delta + \dot{\theta})V - \frac{1}{2}\Gamma U \tag{2.24}$$

$$\dot{V} = -(\Delta + \dot{\theta})U - \frac{1}{2}\Gamma V + \Omega W$$

$$\dot{W} = -\Omega W - \Gamma(W+1)$$

From these equations we can arrive at a particular case, it is when the atom moves very slowly so that the variation in position is very small during the life time of the excited state.($\tau - 1/\Gamma$). In this case we can assume that the atomic system reaches a stationary state in each position, that is $\dot{U} = \dot{V} = \dot{W} = 0$, taking into account this condition, the equations (2.24) it can be solved, therefore we can have the radiation force as follows.

$$\vec{F} = -\frac{\hbar\Gamma\Omega^2\nabla\theta}{4(\Delta+\dot{\theta})^2+\Gamma^2+2\Omega^2} - \frac{\hbar(\Delta+\dot{\theta})\nabla\Omega^2}{4(\Delta+\dot{\theta})^2+\Gamma^2+2\Omega^2} \tag{2.25}$$

The first term of the above equation is called "spontaneous force" or also as the "dispersion force" that is due to absorption and spontaneous emission processes, a certain amount of momentum will be transferred to the atoms by photons. The second term, which is proportional to the gradient of radiation intensity (because $\Omega \propto E \Rightarrow \Omega^2 \propto I$) which corresponds to the so-called "induced force" or "dipole force" coming from the interaction of electromagnetic radiation with the induced electric dipole in the interaction. One of the main differences between these two radiation forces is that the dipole force is based exclusively on the stimulated effects, and it is not saturable compared to the spontaneous force, since it is saturated for high intensities, being $\Gamma\hbar\dot{\theta}/2$ the saturation value.

The equation (2.25) depends explicity on $\theta(R,t)$. For the case of a plane wave $\nabla\theta = -\vec{k}$ and therefore $\nabla\Omega^2 = 0$, in this case the spontaneous force will be the only one present then we will explain in which cooling processes this force will be present. For the case of Gaussian beam $\nabla\theta \neq 0$ here both forces are present, the atom being subject to a longitudinal force (spontaneous force) in the direction of radiation propagation and a transverse force (dipole force) due to the dipole interaction with intensity gradient present in the Gaussian beam.

2.3 Doppler cooling and optical molasses

In order to cool atoms moving in a vapour we need to reduce the velocity propagation of a group of atoms, such as trapping them in the momentum space, a velocity-dependent force is required; $\vec{F}_{scatt} \propto -\vec{v}$. These forces arise from the interaction of an atomic ensemble with the light beam with a detuning near to the resonance of the atomic transition in

combination with the Doppler effect, as was proposed by Hansch and Schawlow in 1975.[27]

As we know, the Doppler effect (or the Doppler shift) is the change in frequency of a wave in relation to an observer who is moving relative to the wave source. In laser cooling and trapping the idea is basically the same. The frequency of the light beam ω (as the wave) felt by the atoms (as the observer) will shifted due to the Doppler effect. The actual detuning represented by $\Delta' = \omega - \omega_0 - \vec{k}.\vec{v}$ will be the actual detuning for a moving atom, where $\Delta = \omega - \omega_0$ is the detuning for an atom at rest.

In this force, the processes that are carried out are absorption and spontaneous emission, each absorption of a photon will produce a recoil in the atom, that is, it will gain a recoil speed $\vec{v}_{recoil} = \hbar\vec{k}/m$ (m = mass of the atom), over a transition time towards an excited state.

Returning to the equation (2.25) the first term that represents the total force is the scattering force (or dispersion force), then we have:

$$\vec{F}_{scatt} = -\frac{\hbar\Gamma\Omega^2\nabla\theta}{4(\Delta + \dot{\theta})^2 + \Gamma^2 + 2\Omega^2} \tag{2.26}$$

For the case of a plane wave $\vec{E}(\vec{r}, t) = E_o cos(\vec{k}.\vec{r} - \omega t)$, where $\Omega = \mu E_o/\hbar = const.$ and $\theta(\vec{r}) = -\vec{k}.\vec{r}$ therefore $\dot{\theta} = -\vec{k}.\dot{\vec{r}}$, and then, the scattering force will be expressed as:

$$\vec{F}_{scatt} = \frac{\hbar\Gamma\Omega^2\vec{k}}{4(\Delta - \vec{k}.\dot{\vec{r}})^2 + \Gamma^2 + 2\Omega^2} \tag{2.27}$$

In a strong field Ω, this force will present a saturation effect:

$$\vec{F}_{sat} = \lim_{\Omega\to\infty} \vec{F}_{scatt} = \frac{1}{2}\Gamma\hbar\vec{k} \tag{2.28}$$

Showing the maximum value of the force in the system.

Now let us see, the behavoir of a cloud of atoms when they are subjected to two counter-propagating beams coming from the same laser and having equal intensity and frequency in the direction z (1D) see figure 9 and in the low intensity regime (where stimulated emission could be neglected). In this configuration, we will see how this force can act as a buffer to the movement of atoms using the equation (2.25), we can find the net force subjected to the atom in motion.

It is clear to think, that for two beams of light in opposite directions acting over an atom, the resulting force will be zero as long as the atom is at rest. However, for atoms with speeds other than zero, there will be an imbalance of forces due to the Doppler effect.[28]

For the case when the atoms present speeds different from zero, they will experience a net force that is proportional to their speed and whose sign depends on the detuning of the light beam. If the light beam frequency is red-detuned, the beam moving opposite to atomic motion is blue-shifted in frequency and hence gets closer to resonance. For the case where the light beam moving in the direction of atoms would be red-shifted in frequency and gets further away from resonance. Thus, atoms scatter more photons from the beam that is opposite to their motion, and this differential scattering results in a net damping force[3] . Thus, the atom undergoes an asymmetric influence by the laser beam depending on the direction of its motion.

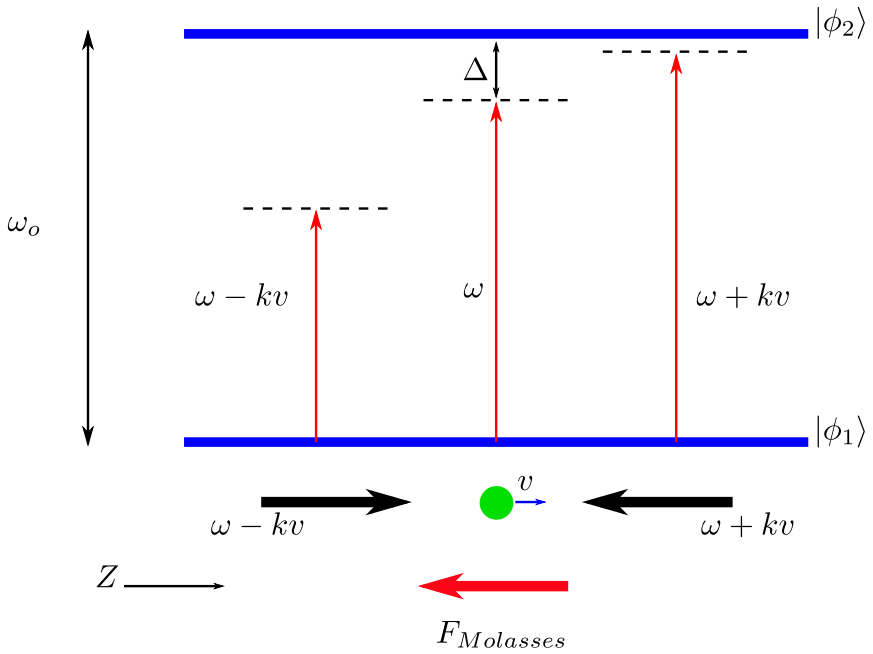

Figure 1 – Optical molasses scheme in one dimension for a two level atom that has a velocity component v along the z-axis.
Source: By the author.

The atoms will scatter more photons from the beam of light that opposes their movement than the beam that goes with them. From the equation obtained in (2.25) using only the force responsible for the speed reduction, that is, the scattering force, we have:

$$\vec{F}_z = \frac{\Gamma\Omega^2\hbar\vec{k}_1}{4(\Delta - \vec{k}_1\vec{v})^2 + \Gamma^2 + 2\Omega^2} + \frac{\Gamma\Omega^2\hbar\vec{k}_2}{4(\Delta - \vec{k}_2\vec{v})^2 + \Gamma^2 + 2\Omega^2} \tag{2.29}$$

Since we are considering a counter-propagating beam of light in the "z" direction, then $|\vec{k}_1| = |\vec{k}_2| = k$, for low intensities, this expression can be expanded in the first-order for $\vec{v}$, and can be written as:

$$F_z(v) \approx \frac{4\hbar k^2(I_z/I_s)(2\Delta/\Gamma)}{[1 + I_z/I_s + (2\Delta/\Gamma)^2]^2} v_z \equiv -\beta v_z \tag{2.30}$$

The Raby frequency Ω is related to the saturation intensity by the saturation parameter, which indicates the probability of finding an atom in the excited state:

$$S = \frac{\Omega^2}{2(\Delta^2 + \Gamma^2/4)} = \frac{I/I_s}{1 + (2\Delta/\Gamma)^2} \tag{2.31}$$

For the red-detuned $\Delta < 0$, the atom will suffer a viscosity of the medium. In this way, this damping force has the role of removing the energy of the atomic system, achieving thus reduce the temperature of the atomic sample. This viscous force is proportional to the speed of the atoms, later we will see another type of force that will depend on space.

The limit of this process is determined by the competition between the energy gained by the spontaneous process and the energy lost due to the viscous force F_z.[29]

$$v^2 = \frac{\hbar\Gamma}{4m} \frac{1 + (2\Delta/\Gamma)^2}{2|\Delta|\Gamma} \tag{2.32}$$

The last equation is related via the equipartition theorem in one dimension given by:

$$T = \frac{mv^2}{k_B} \tag{2.33}$$

Thus

$$T = \frac{\hbar\Gamma}{4k_B} \frac{1 + (2\Delta/\Gamma)^2}{2|\Delta|\Gamma} \tag{2.34}$$

which has a minimum for $\Delta = -\Gamma/2$ (being $\Delta < 0$ to produce the damping force) and leads the Doppler limit for laser cooling:

$$T_D = \frac{\hbar\Gamma}{2k_B} \tag{2.35}$$

T_D is called the Doppler temperature and depends only on the natural linewidth of the excited state. For a potassium ^{39}K and lithium ^{6}Li the minimum attainable temperature in optical molasses will be 140μK and for sodium atoms ^{23}Na corresponds a minimum temperature of 240μK.[30]

2.4 Magneto optical trap

In this section, I briefly review the mechanics of trapping neutral atoms. This mechanism creates a spatially dependent force by exploting the internal structure of the atom by using a static magnetic field.

Optical molasses produces a damping force that is proportional to the velocity. However, atoms in optical molasses still follow a random-walk path due to all the scattering and will eventually diffuse out of the intersection of the overlapping of the light beams, since the lifetime in this configuration is around 0.1s, leaving the optical molasses forever. As we are interested in collecting atoms to have a considerable number and then signal to noise ratio to implement our experiments, it is necessary to add another force that keeps atoms trapped. This is possible by applying a static magnetic field gradient with zero field at the center of the overlap. This creates a force that depends on the position of the atoms and acts as a restoring force. This configuration is known as Magneto Optical Trap (MOT)

If we consider a two-level atom, propagating in one dimension z, the Doppler force exerted by two counter-propagating slightly red-detuned light beams, with circular polarizations and a magnetic quadrupole field of the simple form $\vec{B}(z) = (0, 0, bz)$ with b being the magnetic field gradient and z the spatial coordinate. Applying such linear magnetic field breaks the degeneracy of the hyperfine Zeeman sublevels of the ground and excited states.

$$\Delta E = \mu_B m_{J'} bz \tag{2.36}$$

Here $\mu_B = \frac{e\hbar}{2m_e}$ is the Bohr-magneto and m_J is the projection of the total angular momentum along a specified axis. We can see that for the ground state $J = 0$ the energy

remains undisturbed becasue it has no angular momentum ($l = 0$) while for the excited state $J' = 1$ ($l = 1$) the degeneracy is lifted for $z \neq 0$ according to the energy term mentioned above with $m_{J'} = +1, 0, -1$.

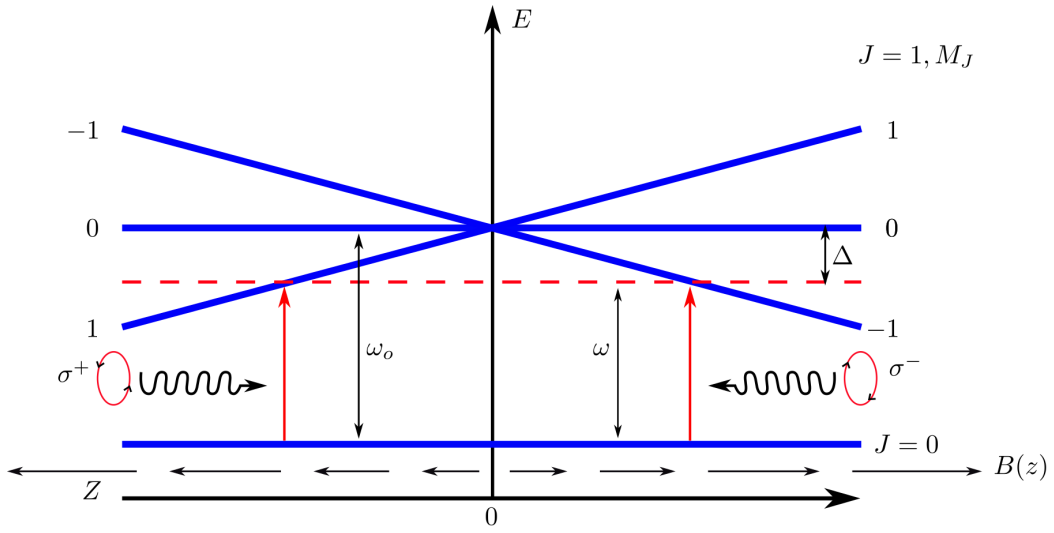

Figure 2 – Mechanism of the MOT in one dimension for two level atom with resonance frequency ω_0 corresponding to the transition $J = 0 \rightarrow J = 1$. Spatial Zeeman splitting of the exited state provides a confinement for atoms in the zeropoint at the center. The frequency ω of the two counter propagating laser beams is red detuned by Δ from resonance. The length of the black arrows represents the strength of the quadrupole magnetic field.

Source: By the author.

To drive the transition $J = 0 \rightarrow |J' = 1, m_{J'} = +1\rangle$ and $J = 0 \rightarrow |J' = 1, m_{J'} = -1\rangle$, right circular polarized (σ^+) light is needed for the first transition or left circular polarized (σ^-) light for the latter, respectively, as a direct consequence of the conservation of angular momentum. If an atom located at position $z > 0$, scatter more photons from the σ^- polarized beam, that from the σ^+ polarized beam since the transition to the $|J' = 1, m_{J'} = -1\rangle$ state is much closer to resonance than $|J' = 1, m_{J'} = +1\rangle$ transition. To atoms located at position $z < 0$ scatters more photons from the σ^+ polarized beam. And at position $z = 0$ will experience no net force at all. This mechanism gives rise to a position dependent force with a direction toward to the center of the trap where $B = 0$.

We can obtain that net force that the atom will experience:

$$F_z = \frac{\hbar k \Gamma \Omega^2}{4} \left[\frac{1}{(\Delta - \omega_D - \frac{\mu_B b z}{\hbar})^2 + \frac{\Gamma^2}{4} + \frac{\Omega^2}{4}} - \frac{1}{(\Delta + \omega_D + \frac{\mu_B b z}{\hbar})^2 + \frac{\Gamma^2}{4} + \frac{\Omega^2}{4}} \right] \tag{2.37}$$

where $w_D = \vec{k}.\vec{v}$

With this new trapping technique (MOT) we are able to obtain a density of atoms in a certain volume. However it will limited by collision processes. If two atoms collide while one of them is in an excited state, there is a posibility that the de-excites into the ground state, heating other atom. Another limitation comes from the spontaneous emitted photons that heat the atoms by causing an k-recoil when they are emitted. These emitted photons can be absorped again by other atoms, leading to a repulsion between the atoms, which poses a limitation on the density that can be created. With these limitations in our cloud of atoms, we will not get the high density needed for Bose Eistein condensates.

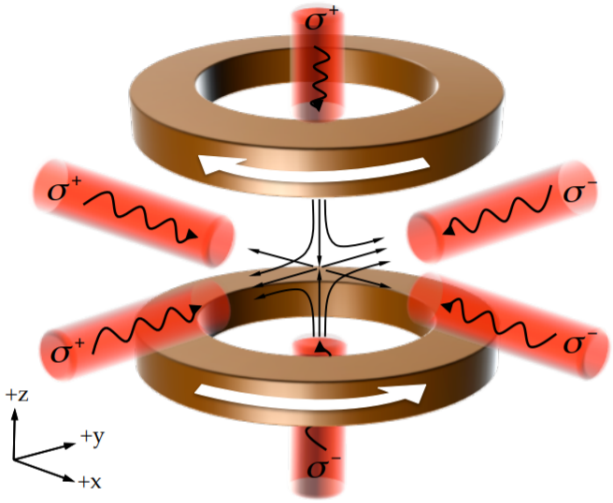

Figure 3 – Magneto optical trap in an anti-Helmholtz configuration, described in a transition $J = 0, 1$. The white arrows indicate the current direction for each coil. In the plane xy, the polarization of the light is σ^-, whereas for the z-axis, the polarization of the light is σ^+.

Source: TAMMUZ.[28]

2.5 Cooling beyond the Doppler limit: sub-Doppler cooling

In the previous sections, we have described the cooling and trapping techniques using the simplest optical transitions, $J_g = 0 \rightarrow J_e = 1$ in order to understand how the system works. This system is limited to the Doppler temperature, which has been demostrated in section 2.3. However, in 1988 experiments have reported temperatures below the Doppler cooling, which were one or two orders of magnitud lower than those predicted by the Doppler cooling theory. Thus, a theory was required in order to explain these sub Doppler temperatures. Therefore groups such as the Ecole Normale in Paris and Stanford University in California reported three new mechanisms known as Sisyphus

cooling, motion-induced orientation and magnetically-induced orientation. In this section, we will discuss briefly two mechanisms that lead to sub-Doppler temperatures, using a more realistic description (multilevel atoms). These mechanisms involve optical pumping among the ground state sublevels, light induced energy shifts of the atomic states and polarization gradients.[31] We will continuing in the low intensity regime (i.e. $\Omega \ll \Gamma$ which leads to $\Gamma_p \ll \Gamma$ where Γ_p is the optical pumping rate).

I would like to clarify that this new type of mechanism (sub-Doppler cooling) does not include new forces; the dipole force and the scattering force are the only ones to act here. However how these forces operate in multilevel atoms which undergo 'optical pumping' that gives rise to new cooling effect.

2.5.1 Sisyphus cooling: lin-perp-lin (1-D model)

In this configuration two counter-propagating laser beams in Lin ⊥ Lin interfere creating standing wave with polarization gradient with a period of $\lambda/2$. Let us assume a two level atom interacting with a light beam with frequency red detuned from the resonance transition $J = 1/2 \rightarrow J = 3/2$. Now the ground state splits in two states $m_J = -1/2, +1/2$ and the excited state are described by the magnetic quantum numbers $m_J = -3/2, -1/2, +1/2, +3/2$. Remenber that the ground level J_g of most atoms, in particular alkali atoms, has non zero angular momentum.

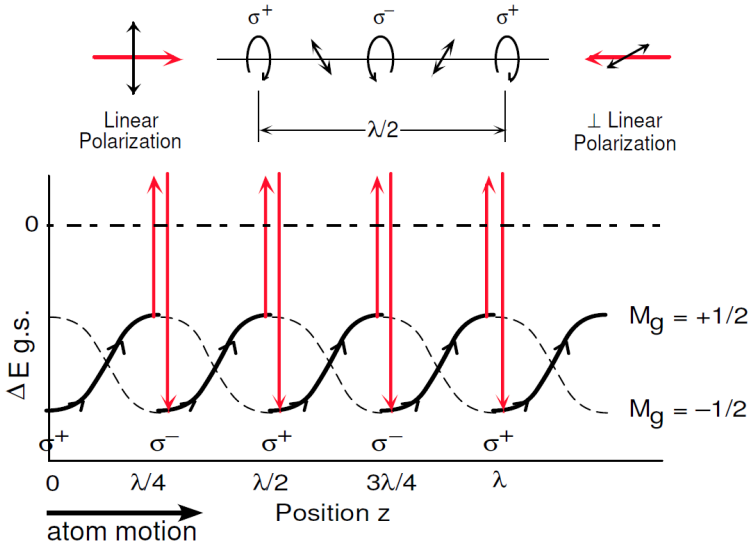

Figure 4 – Schematic of Sisyphus cooling for $J_g = 1/2 \rightarrow J_e = 3/2$ transition in Lin ⊥ Lin configuration. The upper portion shows the polarization set up by the two beams. The lower figure shows the ground state sublevels which are light shifted by the polarization gradient set up.

Source: MARUYAMA.[31]

The interference between these two counterprogating light beams creates a position dependent polarization gradient with a period of $\lambda/2$. The ground state sublevels experience different amounts of light shift depending on the polarization of the light. For σ^+ light couples more strongly to the $m_J = +1/2$ ground state (is shifted three times) than the $m_J = -1/2$ sublevel when the atoms are located at $z = 0$. At $z = \lambda/4$, the resulting polarization gradient changes to σ^- and the atoms must climb up a potential hill, them they are optically pumped to the $m_g = -1/2$ sublevel, and the whole process start all over again. Thus an atom loses kinetic energy twice: first while climbing up the potential hill and second due to optical pumping when it reaches the top of the hill. This process is repeated over multiple cycles until the atom has a kinetic energy smaller than the height of the potential hill itself.

The temperature in this process is determined by equipartition theorem in one dimension $k_B T_f = \frac{D_p}{\beta}$. The fact, this theorem was derived by A. Eistein in his article tittled "On The Theory of Brownian Motion". Here T_f represents the final temperature, D_p and β are the momentum diffusion and friction coefficients respectively. These coefficients are calculated in[32–33] using a semiclassical theory in the regime of low intensity $\Omega_0 \ll \Gamma$ and for small velocities $kv_z \ll \Gamma$. And they are summarized in HOPKINS'S thesis doctor[34] for both cooling schemes. Therefore, the expression for each coefficeint are:

$$\beta \approx -3\hbar k^2 \frac{\Delta}{\Gamma} \tag{2.38}$$

This friction coefficient β is independent to the laser intensity, whereas for the Doppler cooling this coefficient is proportional to the laser intensity. Finally the momentum diffussion coefficient D_p was calculated for large detunings $\Delta >> \Gamma$ is given by:

$$D_p \approx \frac{3\hbar^2 k^2 \Omega_0^2}{8\Gamma} \tag{2.39}$$

This coefficient is a contribution of three process: fluctuations of the momenta of spontaneously emitted photons, Poissonian fluctuactions in the absorption rate and fluctuations in the instantaneous in the dipole force.

Putting the above equation into equation $k_B T_f = \frac{D_p}{\beta}$, will give us the temperature of Sisyphus cooling:

$$k_B T_f = \frac{\hbar \Omega_0^2}{8\Delta} \tag{2.40}$$

As we can notice, from above equation that temperature is directly proportional to the laser intensity and inversely proportional to the laser detuning. The thermal energy $k_B T_f$ is of the order of the light shift ($\hbar\Omega_0^2/4\Delta$).

2.5.2 Corkscrew cooling: σ^+-σ^- (1-D model)

Corkscrew cooling or motion-induced orientation cooling employs two counter-propagating light beams (same wavelenght and frequency) with cicular polarized and orthogonal to each other. In this configuration the resulting polarization is linear everywhere, and rotating in a corkscrew-like manner. The resulting polarization will not induce a light shift because is linear in any position and no forces on the stationary atom. However, this rotating polarization creates an effect, known as motion-induced atomic orientation. To explain this cooling mechanism we need to consider a simple transition $J_g = 1 \rightarrow J_e = 2$.

This effect causes a motion-induced population in the ground state $m_g = 0, \pm 1$. If the atom moves towards a σ^- light beam, the $m_g = -1$ is more populated; if an atom moves towards a σ^+ light beam, the $m_g = +1$ is more populated.

From figure **??**, atom in $m_g = -1$ (for atom at rest) will absorb from σ^- beam with six times higher probability than from σ^+ more photons from σ^- than from σ^+ and the $m_g = -1$ state will be more populated according to Clebhs-Gordan coefficients (square). However, the motion-induced atomic orientation atoms moving towards σ^-, the $m_g = -1$ state will be more populated. This means that the atoms will absorb more probably from the σ^- against which they move.Thus atoms with certain velocity moving in the light field, its optical pumping process lags behind the change in the laser polarization. This lag will produce in a population imbalance resulting from the scattering rate of counter-or co-propagating σ^+ and σ^-.

In this configuration, the friction coefficient β and momentum diffusion coefficient D_p are given by:

$$\beta = \frac{120}{17} \frac{-\Gamma\Delta}{5\Gamma^2 + 4\Delta^2} \hbar k^2 \tag{2.41}$$

This friction coeffcient is for the regime of low intensity and low velocity but for any detuning. And the diffusion coefficient for large detuning $\Delta \ll \Gamma$ is given by:

$$D_p \approx \frac{29\hbar^2 k^2 \Gamma \Omega_0^2}{170\Delta^2} \tag{2.42}$$

Putting this coefficient into the equipartition theorem $k_B T_f = \frac{D_p}{\beta}$, will give us the temperature in this scheme:

$$k_B T_f \approx \frac{\hbar \Omega_0^2}{10\Delta} \tag{2.43}$$

As we can see, the temperature of the Corkscrew cooling is directly proportional to the laser intensity and inversely proportional to the detuning of the laser.

The main difference between these cooling schemes is that Sisyphus cooling relies on the dipole force, whereas the Corkscrew cooling relies on the scattering force. Another important difference between them is the capture velocity, for the case of Sisysphus cooling, this is proportional to the optical pumping rate $kv_v \approx 1/\tau_p$, whereas for the Corkscrew cooling, is proportional to the light shift $kv_z \approx \Omega_0^2/4\Delta$.

2.5.3 Recoil limit

This mechanism of Sisyphus cooling and Corkscrew cooling has a limited. Because the slowest atoms can still abosrbing and emiting photons spontaneously. Each time atoms emits photon λ recoil with momentum $\vec{p} = \hbar\vec{k}$, limiting the lowest temperature that can be reached in this process can be obtained as:

$$k_B T = \frac{p^2}{2m} = \frac{\hbar^2 \vec{k^2}}{2m} \tag{2.44}$$

Then the lowest temperature could be obtained as:

$$T_{recoil} = \frac{\hbar^2 \vec{k^2}}{2mk_B} \tag{2.45}$$

For potassium ^{39}K using D1 line the recoil temperature is 0.41136702μK (theorical) and the corresponding recoil velocity is about 1.33 cm/s.[35] However we can go beyond this limit using another sub-Doppler techinque called gray molasses.

3 THE GRAY MOLASSES COOLING TECHNIQUE

In this chapter, we will discuss the basic principles of the Gray molasses cooling technique on the D1 transition for ^{39}K atoms. This technique was theoretically proposed by [Shahriar *et al.*,[36] Weidemüller *et al* .[37]], and the first experimental realizations were carried out for ^{133}Cs[20,21] and ^{87}Rb[22] atoms, and recently for ^{40}K,[23] ^{87}Rb[24] and ^{23}Na[25] reaching temperatures six times greater than the single photon recoil energy, employing the D2 transition. Nowadays, this cooling technique is widely used to cool the atoms more efficiently by applying light at the D1 line, because in this transition the atoms present a smaller energetic separation of hyperfine levels in the excited states. In this context, the Gray molasses was realized for ^{39}K,[38] ^{40}K,[39] ^{41}K[40] and ^{23}Na,[41] reaching temperatures 6μK, 20μK, 42μK and 6μK respectively. To understand how this mechanism allows us to obtain the lowest temperatures, one has to consider four theoretical concepts. These are the creation of new non-coupled states $|\psi_{NC}\rangle$, the Sisyphus cooling mechanism, the velocity selective coherent population trapping (VSCPT), and the λ-configuration itself.

In the following sections, we start with a description of trivial dark states, non-coupled states and true dark states, continues with the components of the Sisyphus cycle and how it ties together with VSCPT to form the Gray molasses.

3.1 Trivial dark states

I would like to clarify that the term "dark state" could be those atomic states that cannot be excited because the light has either a wrong frequency or the polarization is such that selection rules do not allow a transition to higher state, called trivial dark states or those that are created by a coherent superposition of states through processes known as the two-photon Raman coupling $|\Psi_{NC}\rangle$. In the first case, we can consider the transition $F \rightarrow F' = F$ as shown in figure 5, which is an example for σ^+/σ^- polarization and in this frame the $m_F = 2/m_F = -2$ are trivial dark states because another excitation is forbidden due to the selection rules, so the light can not be coupled to that states and for π polarization the $m_F = 0$ is a trivial dark state as well. The Gray molasses cooling operates on the $F \rightarrow F = F'$ which is our case for ^{39}K or $F \rightarrow F' = F - 1$ for the case of ^{40}K, being these transitions a property for alkali metals operating on the D1 transition.

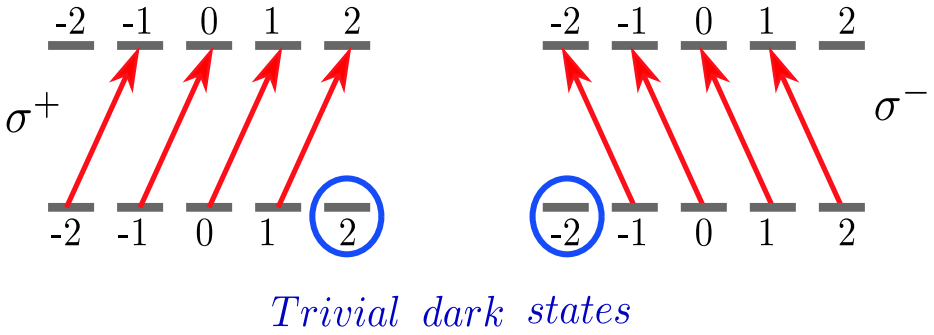

Figure 5 – Trivial dark states for σ^+ and σ^- polarized light for a $F = 2 \rightarrow F' = 2$ optical transition.

Source: By the author.

3.2 Non-coupled states $|\Psi_{NC}\rangle$ and velocity-selective coherent population trapping (VSCPT)

In this section, we will discuss in a briefly way about the (VSCPT) cooling mechanism and how it exceed the single photon recoil limit temperature given by $T_r = \hbar^2 k^2 / 2mk_B$ through the formation of velocity of a selective non-coupled state. These non-coupled states are characterized by a narrow velocity spread around $v = 0$. The main role of this mechanism is to send the atoms towards these non-absorbing states ($|\Psi_{NC}\rangle$, $p \approx 0$), in that manner, we can prevent the atoms with momentum $p < p_r$ from absorbing another photon that could increase their momentum. Once a large number of atoms are pumped into these states (dark states $p = 0$), the temperature of the atomic cloud will reach sub-recoil temperatures, since the temperature is proportional to the width of velocity/momentum distribution.

Now let us have consideration to the formation of non-coupled states. Figure 6 represents a three-level Λ configuration on a $J_g = 1 \rightarrow J_e = 1$ transition interacting with two counter-propagating beams with circular polarization producing the existence of four possible transitions, and one of them being a prohibited transition $|g_0\rangle \rightarrow |e_0\rangle$. The latter transition is not considered in this scheme, since optical pumping empties the $|g_0\rangle$ sub-level. The two-photon Raman processes allow us to transfer atoms from one ground state $|g_{-1}; p - \hbar k\rangle$ to another one $|g_{+1}; p + \hbar k\rangle$, by absorption of σ^+ polarization and stimulated emission produced by σ^- polarization, being $|e_0, p\rangle$ the intermediate excited level. As we can observe, a closed momentum family $F(p) = |g_{-1}, p - \hbar k\rangle, |e_0, p\rangle, |g_{+1}, p + \hbar k\rangle$ can be created for each value of p by absorption-stimulated emission cycles among these three sub-levels.

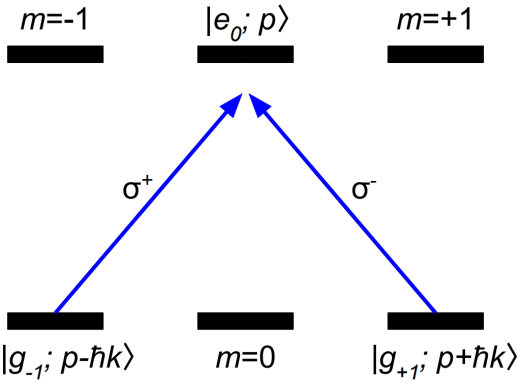

Figure 6 – Magnetic sublevels for a $J_g = 1 \rightarrow J_e = 1$ transition. The atomic states are labeled using two quantum numbers : magnetic quantum number that specifies the internal spin and the z component of the external momentum.
Source: RASTOGI.[3]

In this context, the term ¨coupling¨ will be suitable since we can create a linear combination among these three sub-levels. One of these linear combinations yields a state that has a finite dipole moment with the excited state and hence is coupled to light. The other combination yields a state with a zero dipole moment and hence is non coupled.

The superposition states resulting from the coupling between ground states of a particular momentum family $F(p)$ can be expressed as,[42–43]

$$\Psi_C(p) = \frac{1}{\sqrt{2}}[|g_{-1}; p - \hbar k\rangle + |g_1; p + \hbar k\rangle] \tag{3.1}$$

$$\Psi_{NC}(p) = \frac{1}{\sqrt{2}}[|g_{-1}; p - \hbar k\rangle] - |g_1; p + \hbar k\rangle] \tag{3.2}$$

From equations 3.1 and 3.2 we can demonstrate which one of these states is coupled to the excited state by examining the effect of the coupling Hamiltonian $\hat{H}_{int} = -\hat{\mu}.\vec{E}(z,t)$ on them. We commence analyzing that $\Psi_C(p)$ state trought $\langle e_0, p|H_{int}|\Psi_C(p)\rangle = \frac{\hbar\Omega}{\sqrt{2}}exp(-i\omega t)$, describing a coupling or absorbing state with the excited state whereas for $\Psi_{NC}(p)$ state this coupling $\langle e_0, p|H_{int}|\Psi_{NC}(p)\rangle = 0$ which means that cannot be coupled to the light due to the destructive interference between the transition amplitudes of the component. However, due to the momentum of the atom, the non-coupling state $\Psi_{NC}(p)$ can be coupled to the absorbing Ψ_C state via motional coupling trought the equation of motion given by: $i\hbar\dot{\rho} = [\rho, H]$ resulting a proportionality to kp/m due to the evolution of the bare Hamiltonian and its kinetic energy. However, for $p = 0$, the $\Psi_{NC}(p)$ state will be

a true dark state since the motional coupling vanishes and it will be explained in section 3.5.

This VSCPT mechanism is not limited by the energy of a scattered photon, as is Sisyphus cooling.[44] However, due to imperfections in the polarization field, it can disturb the process and thus reach the limit of temperature. For that reason, in our laboratory we can not surpass or reach to the temperature recoil $T_r = 0.4\mu K$ of ^{39}K.

3.3 D1 transition

The Gray molasses cooling technique is implemented on the D1 transition as was mentioned before since it presents a lesser separation energetic between the excited states in comparison to the (D2) transition. Furthermore we can note from figure 7 that all dipole allowed transitions, concerning their coupling strengths are less than (D2) transition as shown in figure 8. Therefore, according to the equation 2.43 there is a proportionality between the coupling strenghts Ω_{ij}^2 and the temperature T as follows:

From equation 2.43 we can relate the coupling strenghts with the temperature

$$k_B T = \frac{\hbar \Omega_{ij}^2}{10\Delta}. \tag{3.3}$$

In addition, to having a greater energetic separation between their excited states, we can deduce that the (D1) transition is colder than the (D2) transition.

In contrast to the previous section 3.2, where a single laser beam counter-propagating interact, with a $J = 1 \rightarrow J' = 1$ transition, the Gray molasses technique operates on the D1 line involving either an $F \rightarrow F' = F$ or $F \rightarrow F' = F - 1$ transition as shown in figure 7. Furthermore, this cooling technique works under bi-chromatic fields (cooling and repumper), which is necessary to consider all the possible dipole transitions.

As we can observe from figure 7 a wrong polarization can produce one or two trivial dark states for the transitions $F = 2 \rightarrow F' = 2$ and $F = 2 \rightarrow F' = 1$ respectively. These trivial dark states arise for any type of polarization. Futhermore in this configuration, we can create dark states due to the coherent superposition by velocity selective coherent population trapping between $F - 1$ and F levels when the Raman resonance condition is fulfilled.

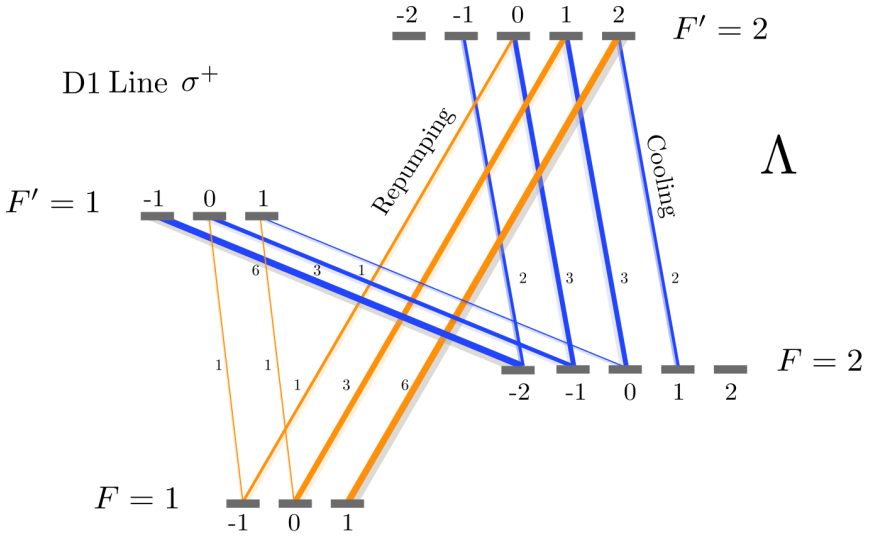

Figure 7 – Transitions strengths for a ^{39}K atoms for σ^+ polarization. The hyperfine states of the (D1) transition from $4^2S_{1/2}$ to $4^2P_{1/2}$ are illustrated.
Source: METCALF.[45]

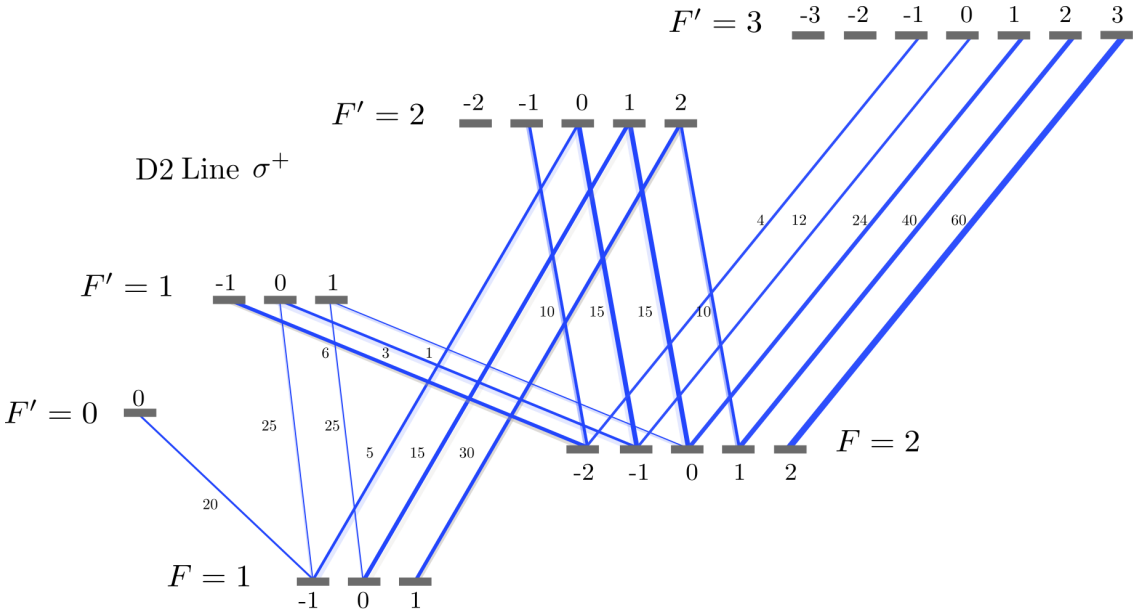

Figure 8 – Transitions strengths for ^{39}K atoms for σ^+ polarization. The hyperfine states of the (D2) transition from $4^2S_{1/2}$ to $4^2P_{3/2}$ are illustrated.
Source:METCALF.[45]

3.4 Principle of Gray molasses

Firstly we examine the effect of the coupled $|\Psi_C\rangle$ and non-coupled $|\Psi_{NC}\rangle$ states onto the atoms in the Gray molasses scheme, which can be described as follows: An atom propagates in a blue detuned $(\delta_1, \delta_2) > 0$ (where δ_1 and δ_2 are the detunings with respect to the excited state $F' = 2$ for the repumping and cooling beams respectively) light field with spatially dependent polarization. The atom-light interaction will divide the ground state into the coupling $|\Psi_C\rangle$ and non-coupling $|\Psi_{NC}\rangle$ states. The main difference between

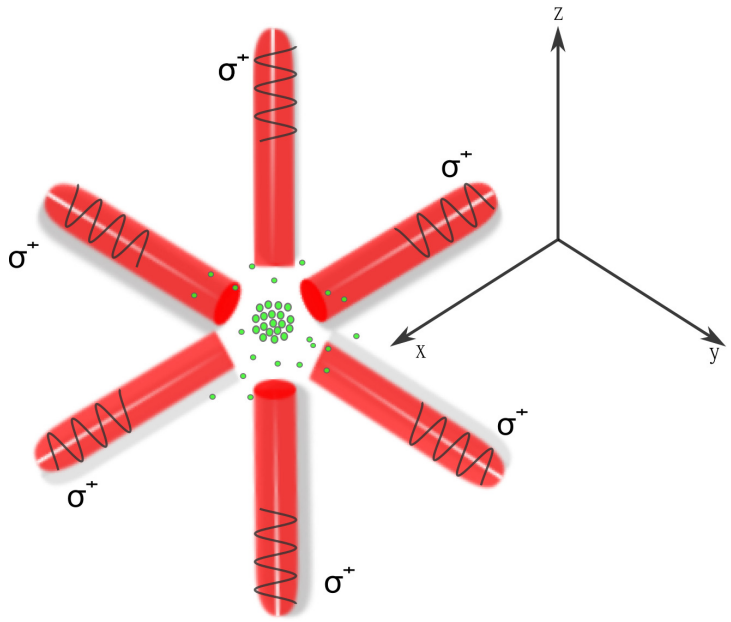

Figure 9 – Atoms in Gray molasses scheme. Three counter-propagating beams covering all three directions. The atoms (green) are located in the center of the intersection.
Source: By the author.

them is that the coupled states $|\Psi_C\rangle$ experience a spatially varying light shift induced by the polarization gradient of the field (discussed later), whereas the non-coupled states remains unshifted. Figure 10(a) shows a schematic picture of one dimensional energy landscape of coupled and non-coupled states. Now let us consider atoms moving through the coupled state along the z-direction. In this state atoms climb the potential of the coupled state converting its kinetic energy to potential energy. Once atom reached the potential hill, it can be pumped to the excited state and via spontaneous emission it decays to the coupled state and undergoes the normal Sisyphus dissipation process. After the spontaneous emission, there are two posibilities, either being coupled to the coupled state $|\Psi_C\rangle$ or it can decay into the dark state as long as the momentum of the atom is $p = 0$. However, atoms with velocity rather than zero $|\Psi_{NC}\rangle$ can be always included in the cooling process until reaching zero velocity, thus $p = 0$ (dark state). The probability of this process is proportional to the velocity of the atom and inversely proportional to the light shift of the $|\Psi_C\rangle$ state (VSCPT).

3.5 Λ configuration and coherent dark state

To explain the emergence of these non-trivial dark states and velocity selective coupling $|\Psi_{NC}\rangle \rightarrow |\Psi_C\rangle$ in a simple scheme, we need to consider a three-level system in Λ

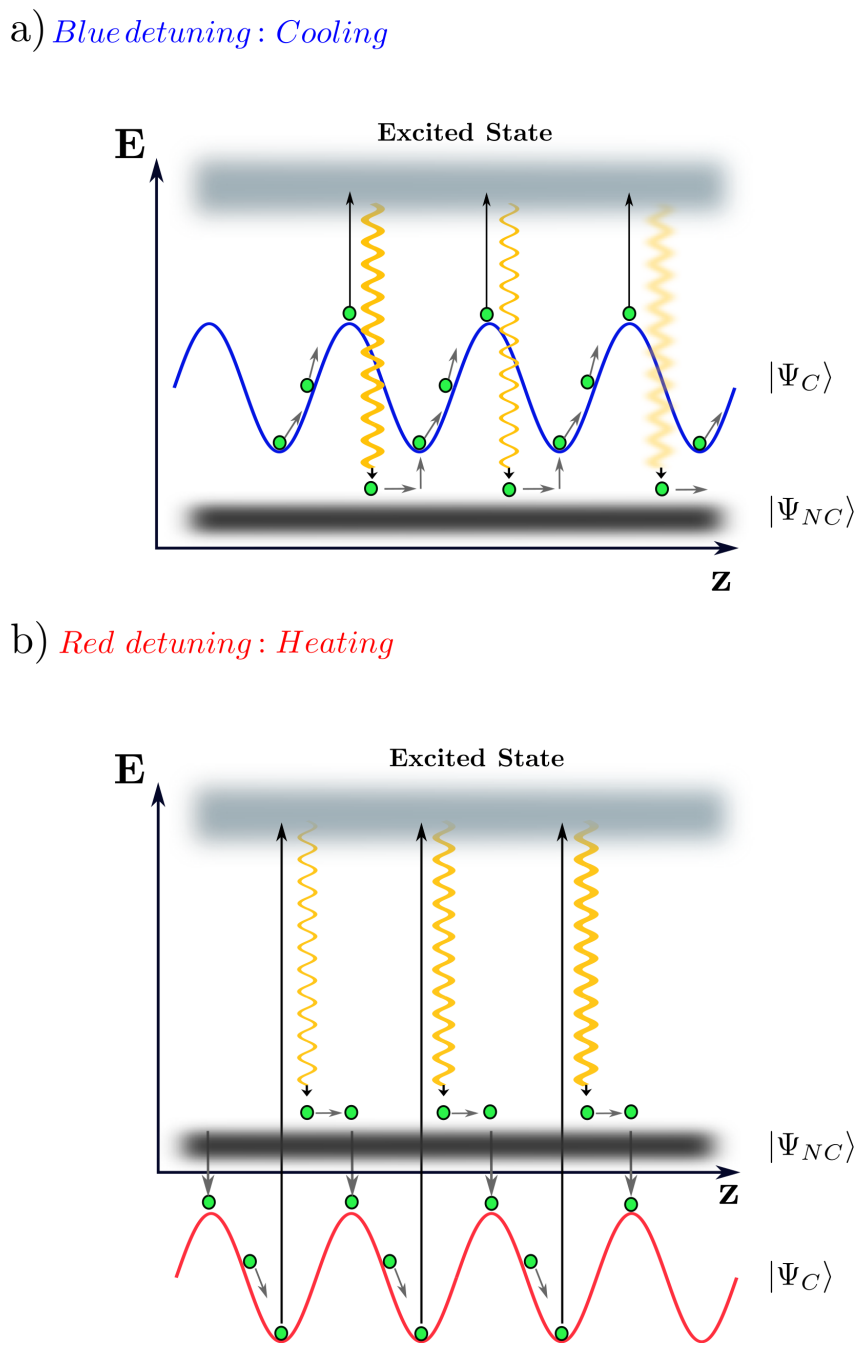

Figure 10 – Working scheme of the Gray molasses cooling technique for different detunings. Source: By the author.

configuration formed by $|^2S_{1/2}, F = 1\rangle = |1\rangle$,$|^2S_{1/2}, F = 2\rangle = |2\rangle$ and $|^2P_{1/2}F' = 2\rangle = |3\rangle$. Figure 11 describes the Λ system with two ground states $|1\rangle$ and $|2\rangle$ and one excited state $|3\rangle$, wih energies ϵ_1 ϵ_2 and ϵ_3 respectively. Each ground state is coupled to the excited state through an oscillator with frequency ω_1 and Raby frequency $\Omega_1 = \Gamma\sqrt{I_1/2I_{sat}}$ (repumping) and the coupling between $|2\rangle$ and $|3\rangle$ is given by an oscillator ω_2 and Raby frequency $\Omega_2 = \Gamma\sqrt{I_2/2I_{sat}}$ (cooling). Another important parameter is the relative detuning

$d = \delta_1 - \delta_2$, see figure 11.

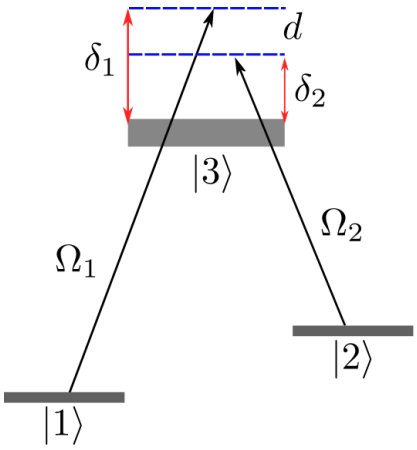

Figure 11 – A three level Λ-system of two ground states $F = 1$ and $F = 2$ of $^2S_{1/2}$ and the excited state $F' = 2$ of $^2P_{1/2}$ of ^{39}K. The repumping beam of frequency ω_1 and detuning δ_1 couples the $F = 1 \rightarrow F' = 2$ transition, whereas the cooling beam of frequency ω_2 and detuning of δ_2 couples the $F = 2 \rightarrow F' = 2$ transition.
Source: By the author.

In this configuration, the simple Hamiltonian (without the kinetic energy) of the system can be described as $H = H_0 + V$, where H_0 is the atom does not interact with the light and another V Hamiltonian that couples with light. In order to obtain the dressed picture of the atom ($|\Psi_C\rangle$ and $|\Psi_{NC}\rangle$), is necessary to diagionalize the Hamiltonian H of the system. First we assume no difference in energy of state $|1\rangle$ and $|2\rangle$ meaning $\epsilon_1 = \epsilon_2$ and the Raman condition is fulfilled $d = 0$. We thus have $\omega_1 = \omega_2$. In the rotating frame the Hamiltonian H can be written as:

$$H = H_o + V = \frac{\hbar}{2}\begin{bmatrix} 0 & 0 & \Omega_1 \\ 0 & 0 & \Omega_2 \\ \Omega_1 & \Omega_2 & -2\delta_1 \end{bmatrix} \tag{3.4}$$

Where:

$$H_0 = -\hbar\delta_1|3\rangle\langle 3| \tag{3.5}$$

and V is the coupling Hamiltonian:

$$V = \left(\frac{\hbar\Omega_1}{2}|3\rangle\langle 1| + \frac{\hbar\Omega_2}{2}|3\rangle\langle 2|\right) + c.c \tag{3.6}$$

After diagonalize the Hamiltonian H, we get two new eigenstates in the dressed state

picture:

$$|\psi_{NC}\rangle = \frac{1}{\sqrt{\Omega_1^2 + \Omega_2^2}}(\Omega_1|1\rangle - \Omega_2|2\rangle) \tag{3.7}$$

$$|\psi_C\rangle = \frac{1}{\sqrt{\Omega_1^2 + \Omega_2^2}}(\Omega_1|1\rangle + \Omega_2|2\rangle) \tag{3.8}$$

As was mentioned before, the state $|\psi_{NC}\rangle$ does not couple with light field, since $V|\psi_{NC}\rangle = 0$, therefore the state $|\psi_{NC}\rangle$ does not experience light shift, whereas for the coupled state we have $\langle 3|V|\psi_C\rangle = \frac{\hbar}{2}\sqrt{\Omega_1^2 + \Omega_2^2}$ meaning that can be coupled to the excited state $|3\rangle$ via the light field. Thus experiences a light shift.

Now the kinetic energy, which is responsible for the coupling between the $|\Psi_C\rangle$ and $|\Psi_{NC}\rangle$ state is considerate to the simple Hamiltonian H. Thus we have a new total Hamiltonian expressed as $H' = \frac{\hat{p}^2}{2m} + H$.[46]

The coupling between the matrix elements and the non-coupled and coupled states is defined in the Arimondo's paper[42] as:

$$\langle\psi_C|H'|\psi_{NC}\rangle = -\hbar\frac{2\Omega_1\Omega_2}{\Omega_1^2 + \Omega_2^2}\frac{kp}{m} \tag{3.9}$$

where p is the momentum of the atom and k is the wave number of the transitions. Here we can see that the coupling depends on the velocity of the atom, since $v = p/m$.[46] Calculate in first order perturbation theory the coupling probability, which gives:

$$P_{|\Psi_{NC}\rangle\to|\Psi_C\rangle} = 2\left(\frac{\Omega_1\Omega_2}{\Omega_1^2 + \Omega_2^2}k\frac{p}{m}\right)^2\delta_1\frac{\delta_1}{\Omega_1^2 + \Omega_2^2} \tag{3.10}$$

This non-adabiatic passage describes the velocity selective coupling of an atom with momentum p from the non-coupled state to the coupled state. This transition probability is proportional to the velocity square, since $v = p/m$. The factor $\frac{\delta_1}{\Omega_1^2+\Omega_2^2}$ describes the inverse of the light shift of the coupled state. δ_1 describes the detuning from resonance, thus the coupling will be strongest at small light shifts and high velocity. This shows that all the slow atoms accumulate in the non-coupled state. The fast atoms are involved in the cooling cycle until the velocity is zero such that the motional coupling vanishes. Therefore, atoms accumulate in dark states, Gray molasses cooling technique could theoretically cool the ensemble even below the recoil temperature. However, the recoil momentum results in

a slight energy mismatch between the atomic states, giving rise to off-resonant light-matter interactions which transfer atoms from dark states back to bright states and ultimately limit the lowest achievable temperatures.

3.6 Cooling scheme of the Gray molasses on the D1 transition of ^{39}K

To implement the Gray molasses cooling we need two light fields detuned above the (D1) transition as is shown in figure 12.

The cooling beam has a frequency ω_2 that corresponds to the transition $|F = 2\rangle \rightarrow |F' = 2\rangle$ with a detuning δ_2. This is:

$$\omega_2 = \omega_{|F=2\rangle \rightarrow |F'=2\rangle} + \delta_2 \tag{3.11}$$

The second beam in this process will be called the repumper beam and will have a frequency ω_1 that corresponds to the transition $|F = 1\rangle \rightarrow |F' = 2\rangle$ with a detuning δ_1. This is:

$$\omega_1 = \omega_{|F=1\rangle \rightarrow |F'=2\rangle} + \delta_1 \tag{3.12}$$

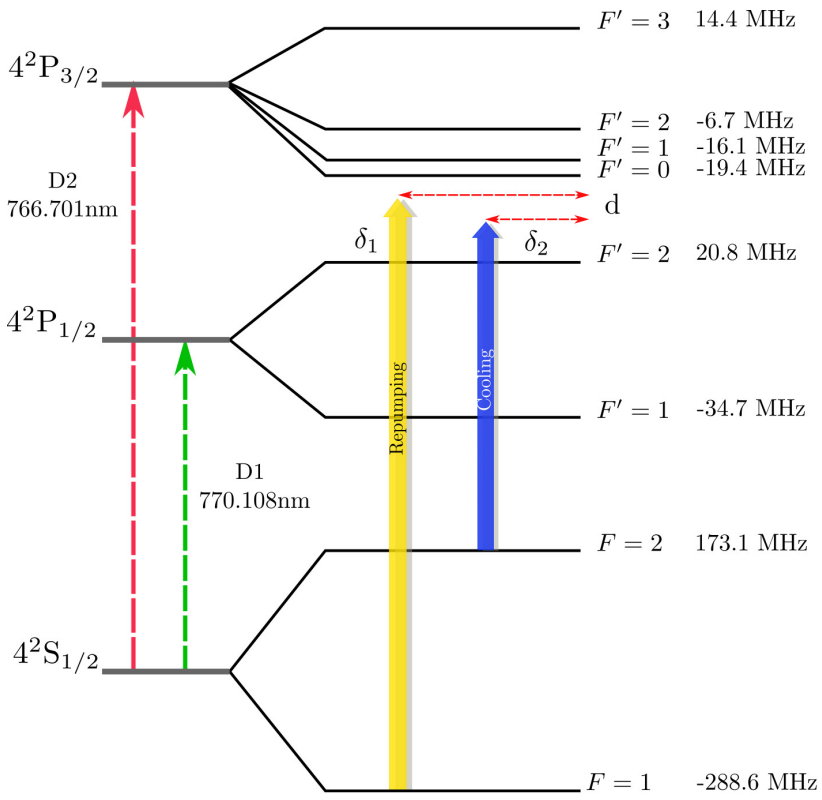

Figure 12 – D1 and D2 transition laser cooling beam detunings.
Source: By the author.

3.7 Raman-resonance condition

The Raman resonance condition is one of the most important parameter in Gray molasses cooling. It has been shown experimentally that even for negatives values of d, we can reach low temperatures. However, the lowest possible temperature is achieved when the Raman condition is fulfilled $d = 0$.

As was explained in ref[3] "when the detuning of the cooling beam δ_2 is smaller than detuning of the repumping beam δ_1, that is to say, $d < 0$. A minimum temperature can be attained, since there is the formation of a weakly coupled state due to the coherence among the m_F sublevels that belong to the same F level. Whereas for $d = 0$, ground hyperfine levels $F = 1$ and $F = 2$ split into bright and (nearly) dark manifolds or (non-coupled states). The dark manifold involves superposition between the m_F sublevels belonging to the two $F = 1$ and $F = 2$ states, creating a coherence betweeen the sublevels of different ground hyperfine levels. The coupling strength of this nearly dark manifold is much weaker than those that are formed by individual cooling and repumping couplings when $d < 0$". Thus when the Raman condition is fulfilled, we can achieve a deep sub-Doppler cooling, since we had created extra non-coupled states. Let us see in the following table 1 all the possible cases of non-coupled and coupled states of the hyperfine structure and the magnetic levels of the (D1) transition for the polarizations σ^+, π and σ^-. For different type of polarization we can create new non-coupled states as is shown in figure 13. Under the influence of σ^+ (left panel) and σ^- (right panel), we can create three additional non-coupled states.

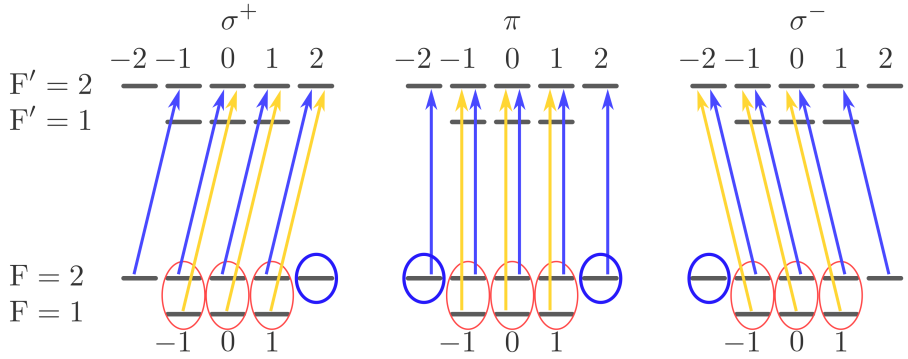

Figure 13 – The magnetic sublevel states of ^{39}K (D1) transition with the allowed transitions depending on the polarization in Gray molasses. Trivial dark states are marked with blue circles and the additional non-coupled states are marked by red elipses.
Source: By the author.

Table 1 – Non-coupled states and coupled states in the dressed state picture of ^{39}K when the Raman condition is fulfilled in the three pure polarization of light σ^+, π and σ^-.

Pol.	**Non-coupled states**	**Coupled states**
σ^+	$\|F=2,m_F=2\rangle$ $\frac{1}{\sqrt{2}}(\|F=1,m_F=-1\rangle) - \|F=2,m_F=-1\rangle)$ $\frac{1}{\sqrt{2}}(\|F=1,m_F=0\rangle) - \|F=2,m_F=0\rangle)$ $\frac{1}{\sqrt{2}}(\|F=1,m_F=1\rangle) - \|F=2,m_F=1\rangle)$	$\|F=2,m_F=-2\rangle$ $\frac{1}{\sqrt{2}}(\|F=1,m_F=-1\rangle) - \|F=2,m_F=-1\rangle)$ $\frac{1}{\sqrt{2}}(\|F=1,m_F=0\rangle) - \|F=2,m_F=0\rangle)$ $\frac{1}{\sqrt{2}}(\|F=1,m_F=1\rangle) - \|F=2,m_F=1\rangle)$
π	$\frac{1}{\sqrt{2}}(\|F=1,m_F=-1\rangle) - \|F=2,m_F=-1\rangle)$ $\frac{1}{\sqrt{2}}(\|F=1,m_F=0\rangle) - \|F=2,m_F=0\rangle)$ $\frac{1}{\sqrt{2}}(\|F=1,m_F=1\rangle) - \|F=2,m_F=1\rangle)$	$\|F=2,m_F=-2\rangle$ $\|F=2,m_F=2\rangle$ $\frac{1}{\sqrt{2}}(\|F=1,m_F=-1\rangle) - \|F=2,m_F=-1\rangle)$ $\frac{1}{\sqrt{2}}(\|F=1,m_F=0\rangle) - \|F=2,m_F=0\rangle)$ $\frac{1}{\sqrt{2}}(\|F=1,m_F=1\rangle) - \|F=2,m_F=1\rangle)$
σ^-	$\|F=2,m_F=-2\rangle$ $\frac{1}{\sqrt{2}}(\|F=1,m_F=-1\rangle) - \|F=2,m_F=-1\rangle)$ $\frac{1}{\sqrt{2}}(\|F=1,m_F=0\rangle) - \|F=2,m_F=0\rangle)$ $\frac{1}{\sqrt{2}}(\|F=1,m_F=1\rangle) - \|F=2,m_F=1\rangle)$	$\|F=2,m_F=2\rangle$ $\frac{1}{\sqrt{2}}(\|F=1,m_F=-1\rangle) - \|F=2,m_F=-1\rangle)$ $\frac{1}{\sqrt{2}}(\|F=1,m_F=0\rangle) - \|F=2,m_F=0\rangle)$ $\frac{1}{\sqrt{2}}(\|F=1,m_F=1\rangle) - \|F=2,m_F=1\rangle)$

Source: Adapted from SHAMMOUT.[47]

4 EXPERIMENTAL SETUP

In this chapter we will describe in a briefly way our compact and versatile NaK experiment built by our group [Castilho *et al.*,[48] Penafiel *et al.*[49]], with the finality to obtain the best performace of Na-K bosonic mixtures.

Our laboratory consist of two optical tables, one of them with the vacuum system composed by three chambers where the light-atom and magnetic field interactions are carried out. And the last one is the optical system where the optical parameters such as frequency, polarization and intensity for each laser system is prepared and optmized.

4.1 The vacuum system

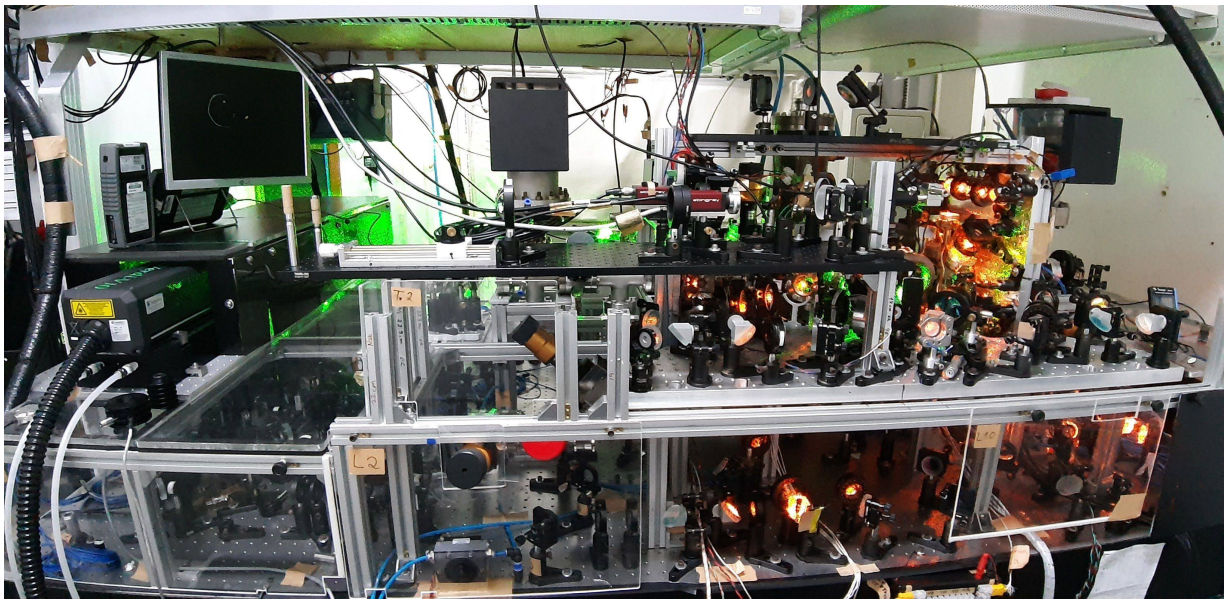

Figure 14 – Optical table where the vacuum system is installled.
Source: By the author.

Figure 14 shows us the optical table of the vacuum system, where all the cooling and trapping techniques take a place, such as optical molasses, MOT-2D, MOT-3D, Hybrid D1-D2 compressed-MOT, Gray molasses, Optical Dipole Trap (ODT), Magnetic Trap (MT), Bose-Einstein condensate (BEC) and other processes that are being studied.

The vacuum system consists of three stainless steel chambers $316L^3$ two of them called "High Vacuum System" (under a pressure of $P \approx 10^{-9}$ Torr), where the processes for capturing atoms from the ovens take place, both for potassium (left side) and for sodium

(right side). The third one (central chamber) or also called science chamber, works under a pressure of $P \approx 10^{-11} - 10^{-12}$ Torr, and it is known commercially as "Ultra High Vacuum" (UHV).

The "High Vacuum System" (HVS) chambers are intended for the use of 2D-MOTs of each atomic species independently. The atomic species come from ovens that produce atomic flow of each atomic species, this will go to one of the 2D-MOTs chambers, both for Potassium and for Sodium. In the case of Potassium-39, the oven temperature is approximately 120°C, since this will be the substance to be studied here.

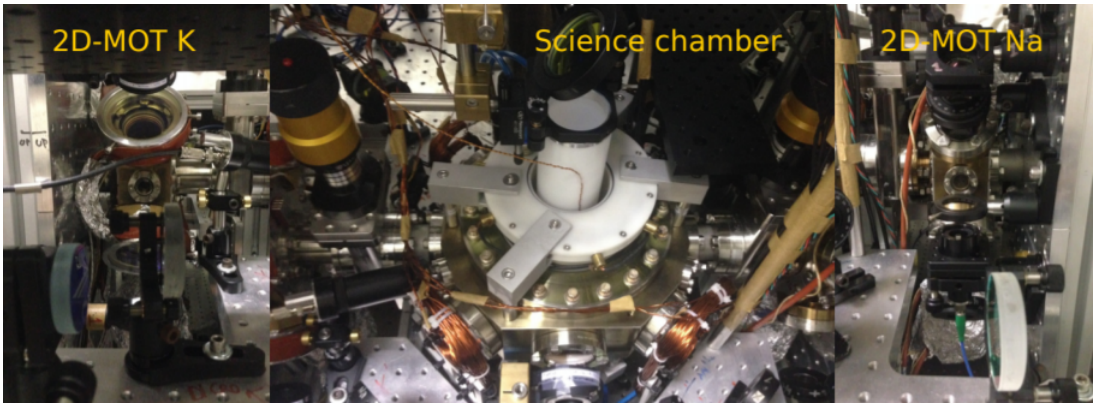

Figure 15 – Vacuum system made up of sections: The first one on the left side shows one of the chambers (HVS) for the 2D-MOT K process. In the center, the chamber (UHV) or science chamber is shown. The last one on the right side shows one of the cameras (HVS) for the 2D-MOT Na process.
Source: Adapted from CASTILHO.[50]

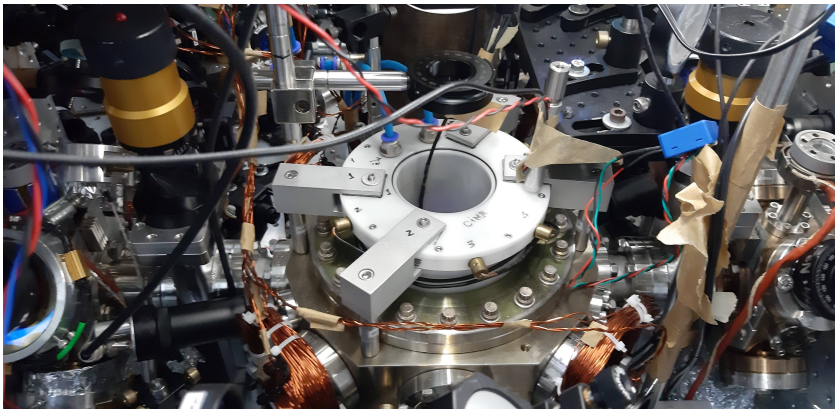

Figure 16 – On the top of Science Chamber we have the upper coil of quadrupole field.
Source: By the author.

Potasssium atoms collected from the 2D-MOT are pushed, by a laser beam, to the Science Chamber where the experiment take place. In this science chamber the overlapping of the 3 perpendicularly configured laser beams takes place, where the atoms are traped

and submited to optical molasses, in addition of this configuration, we have a pair of colis, which are water cooled using an extenal support. In addition to these quadrupole coils, we use three pairs of coils, which helps to compensate minor magnetic field variation.

4.2 Optical system

In this section, we will present all our optical resources used in each stage until to get Gray molasses process, our goal in this work. We have a complete set of lasers and components able to produce all frequencies on each stage of the time sequence of the experiment. Once the lasers are optimized, the beams are carried out through optical fibers to the vacuum system. We have used commertial lasers from Toptica, model TA. In the following subsections, we will describe them.

4.2.1 Lasers on D2 line

This transition is nominally closed meaning that atoms will continue to scatter light through many absorption and emission cycles. To work with this line, we use two Toptica lasers TA-pro centred at $\lambda = 767$nm. One of the lasers is used to perform a cooling transition from $|F = 2\rangle \rightarrow |F' = 3\rangle$ during the laser cooling. However, the rare off-resonant excitation to the $|F' = 2\rangle$ excited state does the atom decay to the $|F' = 1\rangle$ by the selection rules, then the atoms in that state are removed from the cycling transition and are no longer cooled. Consequently, a repumping beam is required to pump the atoms into the cooling cycle, this is the role of our second laser, which will act on $|F = 1\rangle \rightarrow |F' = 2\rangle$ transition, which ensures that the atoms stays in the cycle. And in order to have the best efficient laser cooling we need that the repumping laser be stronger than the cooling laser. The frequencies for each laser is obtained by locking it with respect to the dispersion signal generated from the absorption signal by using saturated absorption spectroscopy (SAS) technique. The lock in frequency is obtained by a module called Digilock from the Toptica laser, using a software.

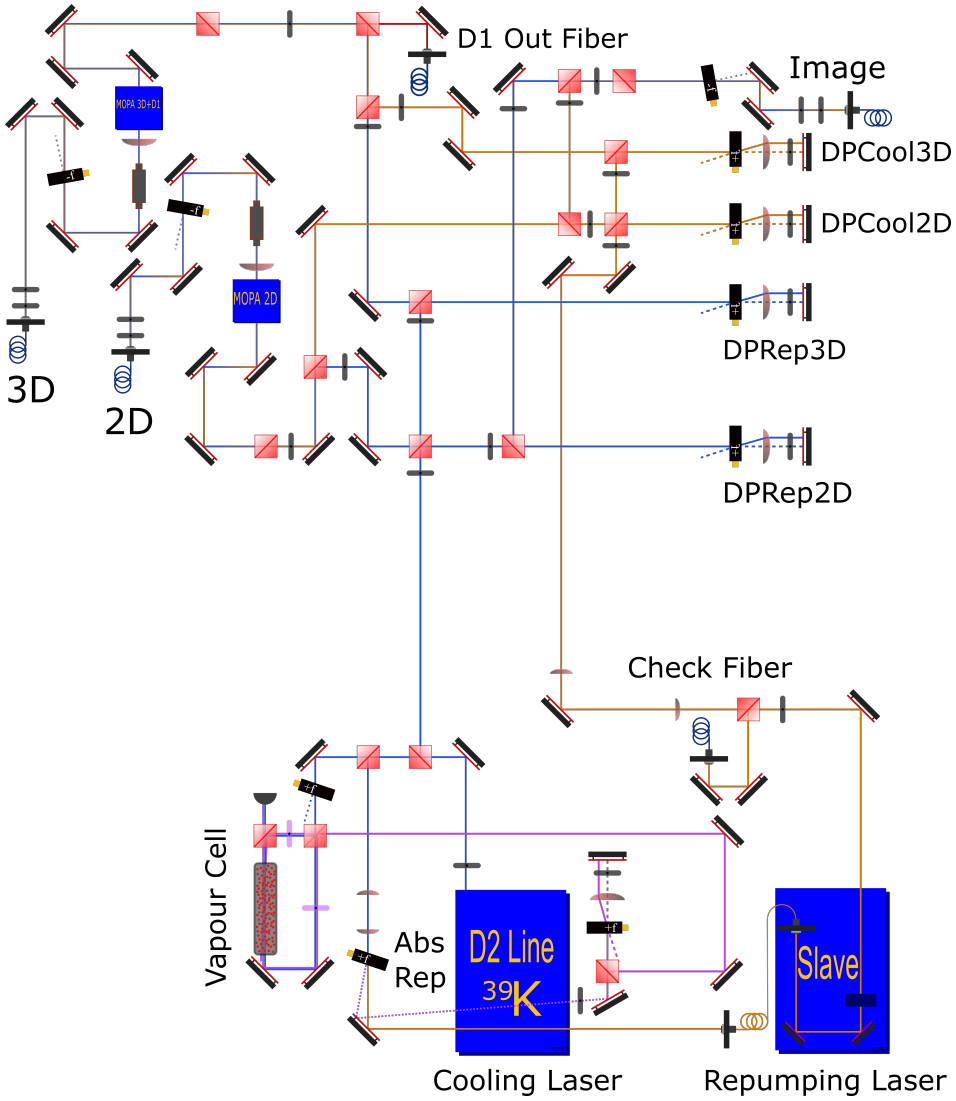

Figure 17 – Laser system for the generation D2 beams.
Source: By the author.

Figure 17 represents the laser system for generation D2 beams. In this laser system, the total power is supplied by a TA TOPTICA laser, part of the total power is sending to the saturated absorption spectroscopy "SAS" technique of the D2 line for potassium ^{39}K. The remaining power is sent to the acoustic optical modulator (AOM) with (+265 MHz) producing a shift in frequency and in this manner we can generate the repumping light. The repumping light is sent towards another TA TOPTICA laser which amplifies the power until 1W.Thus, we have two laser beams (cooling and repumping) with 1W of power for each one. Both laser beams are sending to a double passage to generate the 2D light.

Both light beams are in a superposition configuration and together are sent towards a master optical power amplifier (MOPA) before getting into the 2D chamber. In the same

way, this occurs to produce the MOT 3D.

4.2.2 Lasers on D1 line

As we can see in figure 12, the narrow hyperfine structure of the $4^2P_{3/2}$ excited states will not allow us to use sub-Doppler cooling technique. However, it could be possible if we use near-UV narrow linewidth transitions as was reported in[51] reaching 24μK using the D2 line, but it has no commercial avavility. Gray molasses has a large commercial availability of near-IR light and optics. This cooling technique works on the $|4^2S_{1/2}\rangle \rightarrow |4^2P_{1/2}\rangle$ centred at 770 nm transition (allowing us to get close to the photon recoil limit 0.4μK.[35] To get closer to this theorical limit, we use 200mW to generate $|4^2S_{1/2}, F = 2\rangle \rightarrow |4^2P_{1/2}, F' = 2\rangle$ D1 cooling light and $|4^2S_{1/2}, F = 1\rangle \rightarrow |4^2P_{1/2}, F' = 2\rangle$ D1 repumper light.

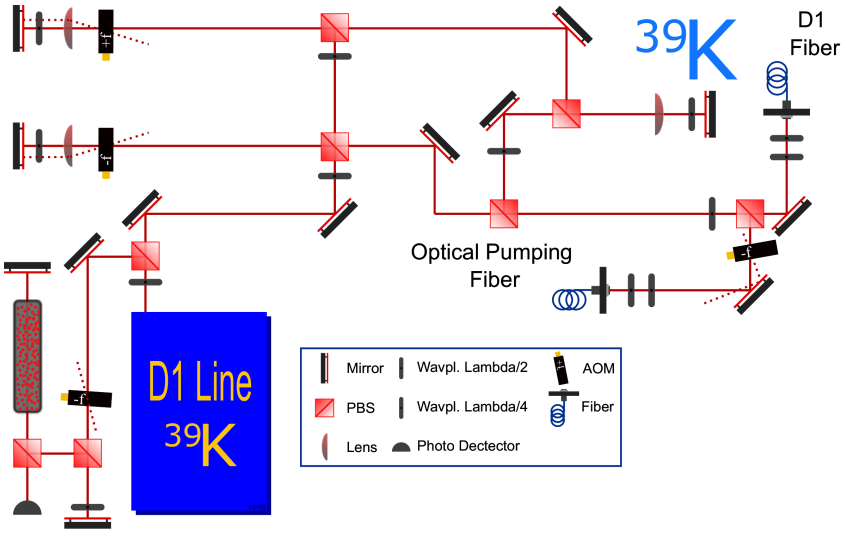

Figure 18 – Laser system for the generation D1 beams.
Source: By the author.

Figure 18 represents the laser system for generation D1 beams. To generate the light necessary to produce the Gray molasses cooling technique, we need a different laser since the difference in frequency between the D2 line and the D1 line is approximately 0.6nm being impossible to produce the D1 line using the D2 line. In this case we a TOPTICA TA PRO whit a total power of 1.2W. This total power will be divided in two double passages. Each double passage will produce the cooling (-110 MHz) and repumping (+119 MHz) light for the Gray molasses. The laser is locking in C.O-C.O (crossover-crossover) of the D1 line for ^{39}K. Both light beams are in a superposition configuration, and they together are sent to MOPA 3D. After the MOPA 3D, both getting into the D2 line in the same path to the science chamber.

4.3 The absorption image technique

In this section, we will see how we are able to extract the atom number and the temperature of our sample of cold atoms, by using the absorption imaging system technique. This technique consists of illuminating the atoms with a resonant light beam. Then, the atomic cloud attenuates the resonant light beam due to absorption, producing a shadow in the beam, allowing us to obtain the dimensions and the geometry of the cloud. For an inhomogenous medium this technique is governed by the Lambert Beer's law, given by[52]

$$I(x,y) = I_0(x,y)e^{-\sigma \int n(x,y,z)dz} \tag{4.1}$$

where $I(x,y)$ and $I_0(x,y)$ represent the transmitted and incident light intensities propagating in an inhomogenous absorbing medium along $\hat{z}$ direction throught an absorptive medium with a spatial density $n(x,y,z)$ or the density profile of the gas and σ is the absorption cross-section of photons.

It can be experimentally evaluated by inverting equation (4.1):

$$\rho(x,y) = -\frac{1}{\sigma} ln \frac{I(x,y)}{I_0(x,y)} = \int n(x,y,z)dz \tag{4.2}$$

The equation above show us that relation between those beam is a density profile integrated along the beam propagation direction $\rho(x,y)$. This is knowm as normalized absorption imaging. Since the trapped gasses usually have a very well defined symmetry we actually can obtain of the physical information of the cloud from this measurement.

In cold atomic experiments this comparison is done by capturing three images frames: a shadow frame $I_s(x,y)$ with atoms and probe light, a light frame $I_L(x,y)$ without atoms and with probe light, and finally we obtain an image without atoms nor probe light to account for the intrinsic noise of the camera and also to eliminate the light presented in the background named as "dark" image, I_d. Hence, the 2D density profile is given by

$$\rho(x,y) = -\frac{1}{\sigma} ln \left(\frac{I_s(x,y) - I_d(x,y)}{I_L(x,y) - I_d(x,y)} \right) = \int n(x,y,z)dz \tag{4.3}$$

From the above equation, we can extract the number of atoms of our cloud by integrating 2D profile.

$$N = \int \rho(x, y) dx dy \tag{4.4}$$

This technique normally is used to obtain data from MOT (or from a conservative trap) and letting them freely expand fall in the direction of gravity during a fixed time called "TOF". To avoid saturation effects due to the high densities of trapped atomic cloud. During the TOF, the atomic cloud will assume an isotropic Gaussian density profile[50]

$$\rho_T(x, y) = \frac{N_{at}}{2\pi\sigma_x\sigma_y} exp\left(-\frac{1}{2}\left[\frac{(x - x_0)^2}{\sigma_x^2} + \frac{(y - y_0)^2}{\sigma_y^2}\right]\right), \tag{4.5}$$

where N_{at} is the number of atoms, $\vec{r}_0 = (x_0, y_0, z_0)$ is the trap centre and σ_i $(i = x, y)$ are the Gaussian widths along $\hat{x}$ and $\hat{y}$.

In the NaK experiment we use two system of imaging, one in the vertical axis, where we can follow the position of the clouds to be trapped at the Plug and Optical Dipole Trap (ODT). And other system as a horizontal imaging with two different magnifications due to the size of the atomic cloud ((2) $M_{MOT} = 0.5$ and (1) $M_{Nak} = 1.6$). We use a CCD camera from Allied Vison model Stingray F-145 is used to capture the images that compose the normalized absorption image.

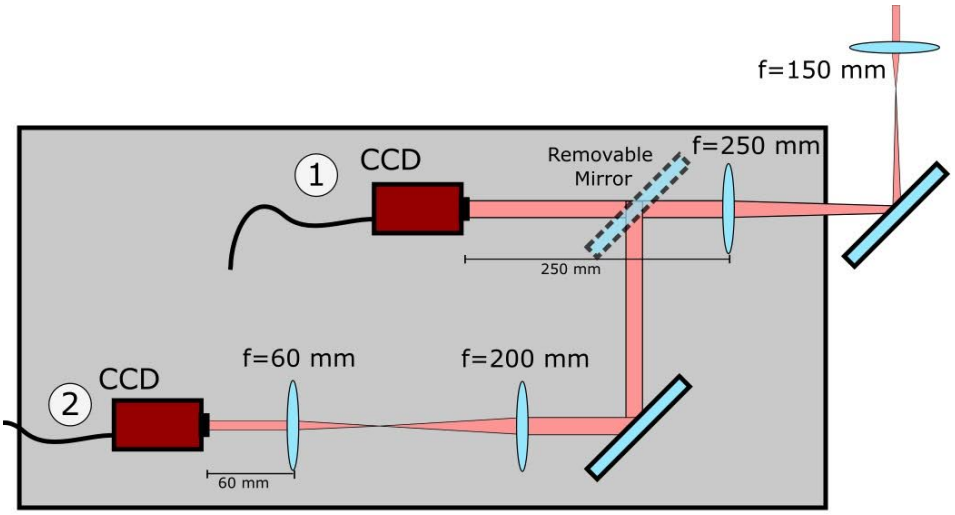

Figure 19 – Illustration of the configuration of the image table. There we can choose between two magnifications to observe our cloud of atoms in the horizontal plane x-y.
Source: MAZO.[53]

4.4 Time sequence of the experiment

In this section, we will present all steps to porduce the best samples at end of the process since the 2D MOT to our Gray molasses. Below we have a typical diagram of the process and its time sequence.

In the next sub sections we will present each step with its details.

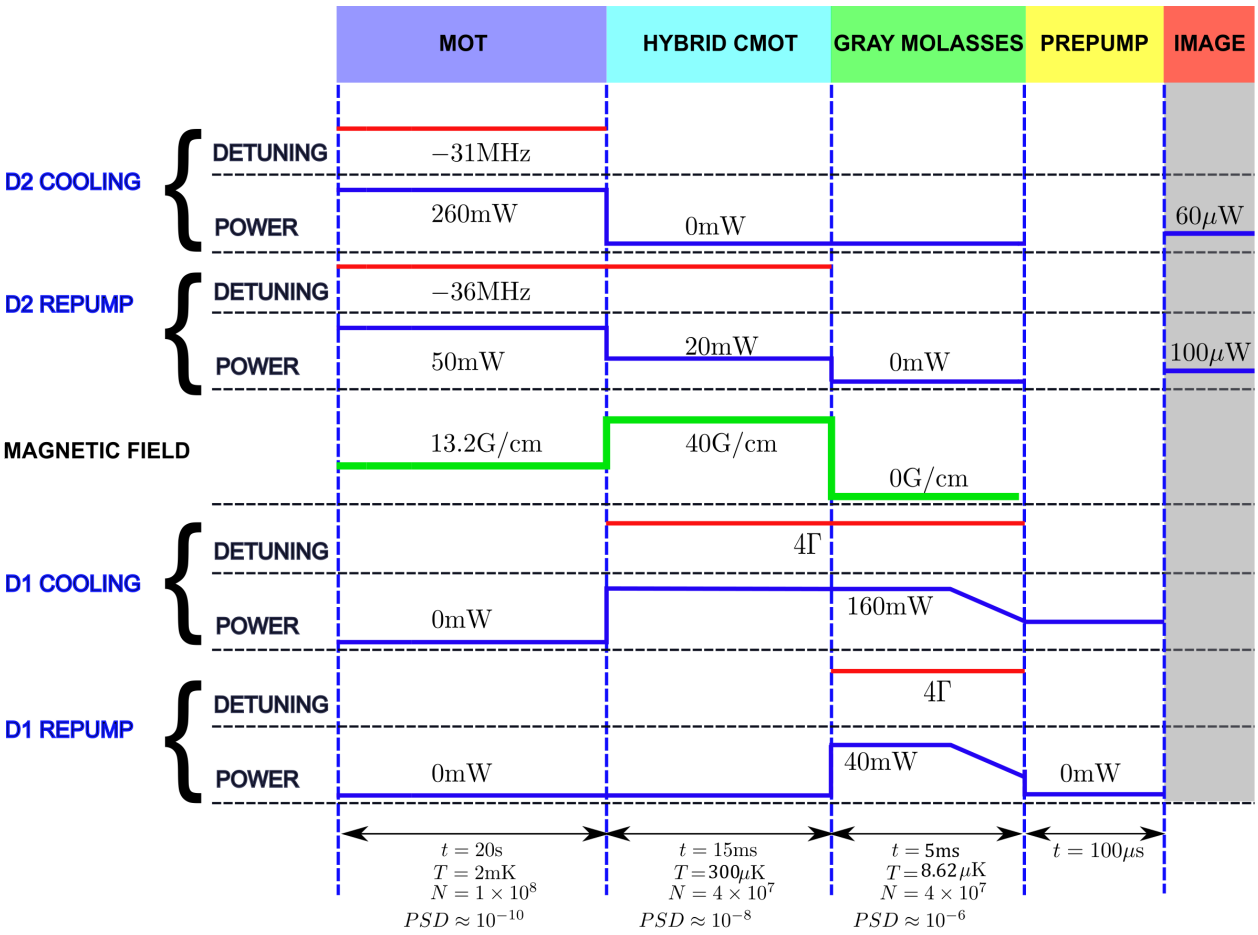

Figure 20 – Experimental sequence with the magnetic field and light of each step.
Source: By the author

4.4.1 Loading of magneto optical trap

As we mentioned previously, the 2D-MOT camera will be the first to receive the atoms from the oven, in this camera it will use two beams of light, one being cooling and the other one being repumping. Both generated in line D2, the cooling will take place in the transition $|4S_{1/2}, F = 2\rangle \rightarrow |4P_{3/2}, F' = 3\rangle$ and the repumping $|4S_{1/2}, F = 1\rangle \rightarrow |4P_{3/2}, F' = 2\rangle$. These light beams are transmitted by optical fibers and overlap perpendicularly in the center of the 2D camera with a polarization $\sigma^+ - \sigma^-$ tuned to red and a magnetic field, allowing to capture the atoms in both directions in the center of the

trap. A red detuned push light beam will push the atoms towards the 3D-MOT chamber, in order to improve the flow of atoms approximately 1×10^8 atoms/s. In this 2D-MOT camera the parameters are always optimized to increase the number of atoms in 3D-MOT.

In our science chamber on 3D-MOT, is necessary to plot the loading curve of the MOT which is the number of atoms trapped as a function of time, which is obtained by the fluorescence of the cloud of atoms and detected by a photodetector. With this technique the number of atoms in the 3D-MOT is around 1×10^8 being enough to obtain the two-species BEC by sympathetic cooling with sodium atoms.

Table 2 – Light detuning and power for the MOT stage

Light	Detuning (MHz)	Power (mW)
Repumper 3D	-36	50
Cooling 3D	-31	260
Cooling 2D	-21	150
Repumper 2D	-18	150
Push (cooling+repumper)	-39	0.26

Source: By the author.

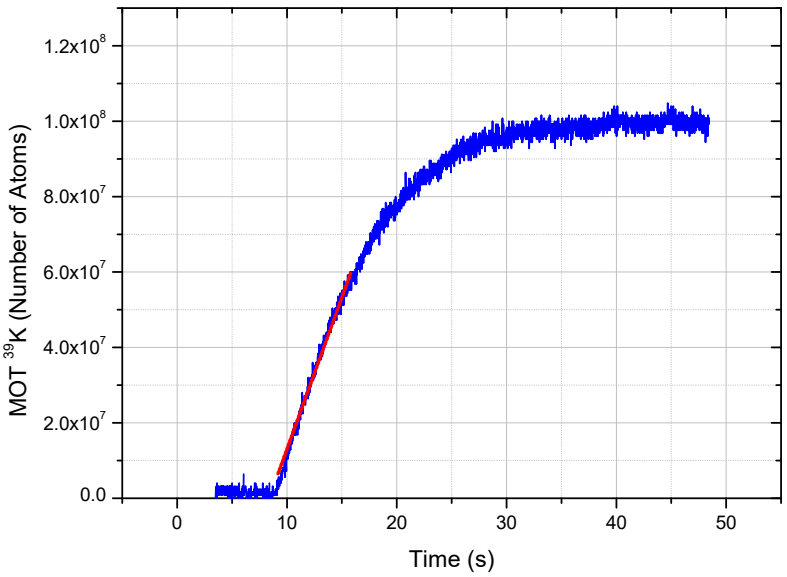

Figure 21 – ^{39}K 3D-MOT loading as a function of time. The 3D-MOT loading rate proportional to the 2D-MOT atomic flux can be obtained by performing a linear adjust at the initial part of the 3D-MOT loading curve (red curve) for which we obtained $L = 1.33 \times 10^7$ atoms/s, being L the atomic flux.

Source: By the author.

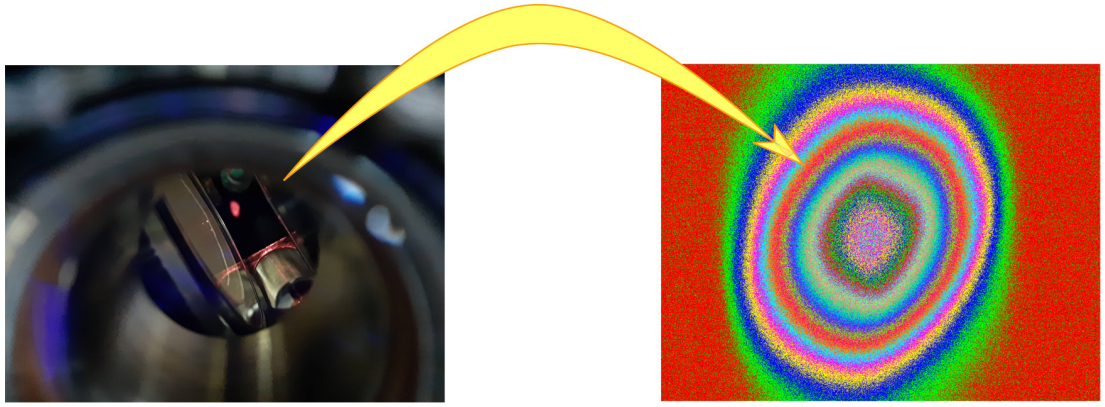

(a) (b)

Figure 22 – (a) The red cloud shows the fluorescence of potassium atoms in the science chamber. (b) Image of the ^{39}K 3D-MOT, captured with a CCD camera Allied Vision model Stingray F-145.

Source: By the author.

The MOT stage will start with 13.2 G/cm and will put a limit on how many atoms are cooled in subsequents steps.

After the MOT stage, we perform a hybrid D1-D2 CMOT stage in order to reduce the temperature of 2mK. In this stage the gradient of the magnetic field is increased and the frequencies are changed lightly. Here the cooling light D2 is turned off and the remaining the repumping light D2 is combined with the cooling light D1 for a short time 15 ms with 40 G/cm. This is performed to obtain the better matching between the size cloud of atoms and the volume of the quadrupole magnetic trap.

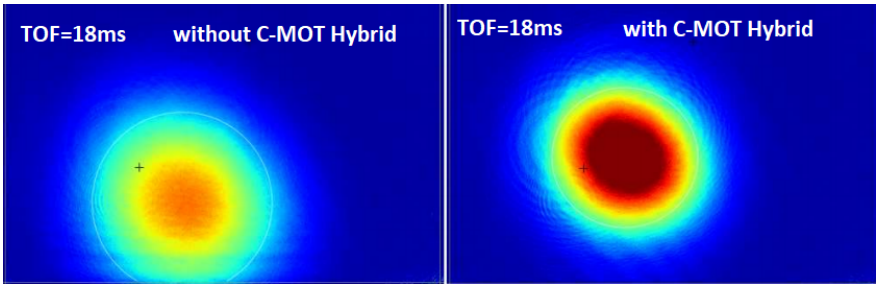

Figure 23 – Hybrid C-MOT. Left: The atomic cloud without compressed MOT.Right: The atomic cloud with compressed MOT.

Source: By the author.

After this stage, Gray molasses starts to work without a magnetic field and the repumper light D2 is replaced by the repumping light D1, leaving the atoms expand in the (D1) light field. In this pre cool stage, there is a loss of atoms, we keep the number of atoms 4×10^7 and the temperature was 800μK.

4.4.2 Imaging procedure for ^{39}K

As discussed before at section 4.3 in order to obtain a image of our atomic cloud, three images are taken.

After the prepump stage, we need to transfer the atoms from $F = 1$ to $F' = 2$ by a 60μs pulse of repump light and the camera stars recording the first image with atoms. The second image without atoms has a similar procedure to the previous one, only without the need for the pumping light.

The last image "dark image" is taken after 100ms and the camera will record by 110μs. To see more specific details see figure 24.

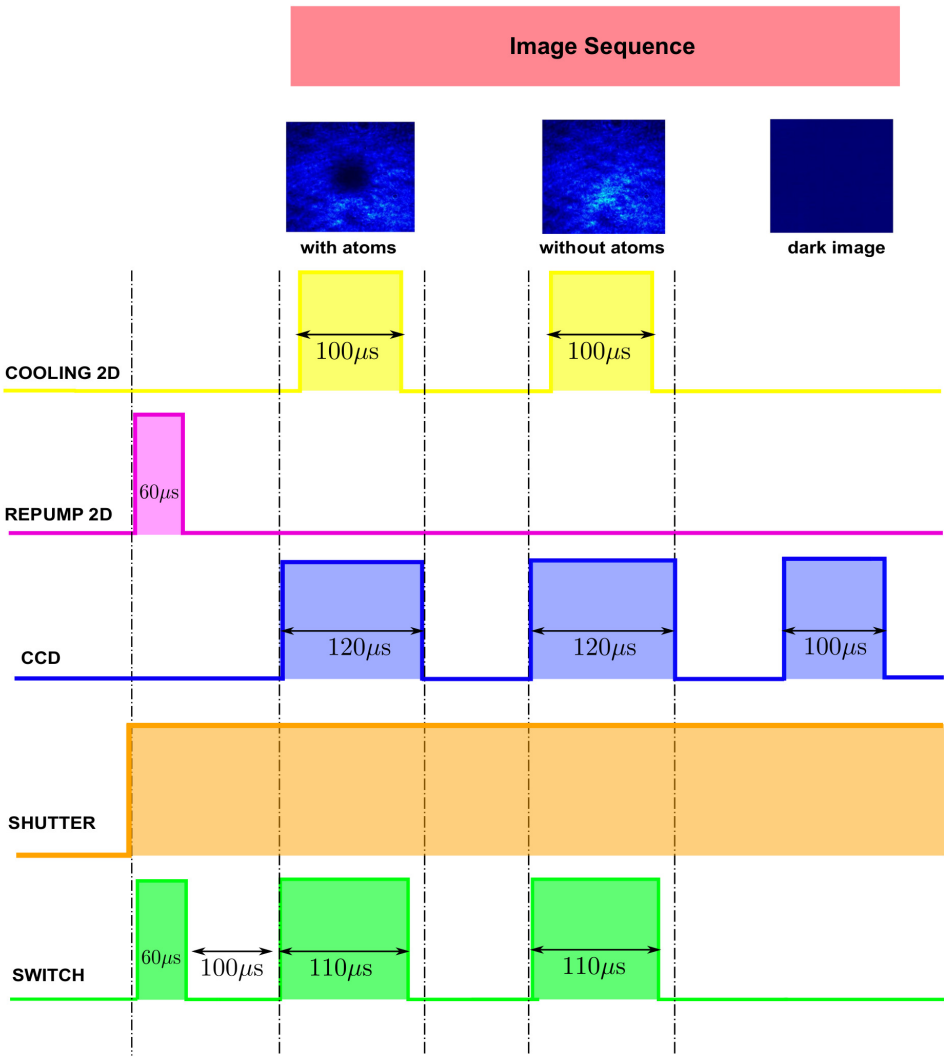

Figure 24 – Sequence image for 39K.
Source: By the author.

The images shown at the top of the image sequence are produced in a CCD camera (Charged-Coupled Device) using a system-design platform (LabVIEW) and a programing language (Phyton).

Once the dark image is finished, the image with and without the atoms goes through an image normalization as shown in figure 25 in order to obtain the normalized image of our atomic cloud.

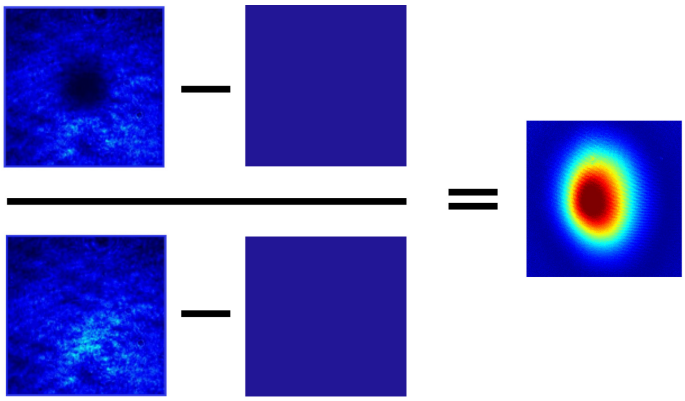

Figure 25 – Imaging processing to obtain the normalized absorption image of the atoms after the Gray molasses stage.
Source: By the author.

4.5 Measurement of temperature and number of atoms in gray molasses

In this section, we will see how we get the temperature and the number of atoms in each stage of pre-cooling by using the time of flight technique TOF.

TOF consists in letting the atoms to expand ballistically without any magnetic field (free expansion) and follow its spatiotemporal evolution. We have two ways to analize that expansion. One by absorption signal, using a probe laser beam through the falling and expanding cloud. This technique is used by its simplicity, reliability temperatures, even being a destructive technique.

As mentioned before in section 4.3 during the TOF, the atomic cloud will assume an isotropic Guassian density profile. The velocity of the expansion is related to the temperature of the atomic cloud throught the energy equipartition theorem in one dimension, given by:

$$\frac{1}{2}k_B T = \frac{1}{2}mv^2 \tag{4.6}$$

m represents the mass of the atom ($6.492424889\times10^{-26}$Kg for K atoms), k_B is the

Boltzmann constant, T is the temperature of the atomic cloud and v is the expansion velocity which is given by:

$$v = \frac{d\sigma_x(t)}{dt} \tag{4.7}$$

Applying this for any two arbitrary time of flight image:

$$T = \frac{\sigma_x(t_2)^2 - \sigma_x(t_1)^2}{t_2^2 - t_1^2}\left(\frac{m}{k_B}\right) \tag{4.8}$$

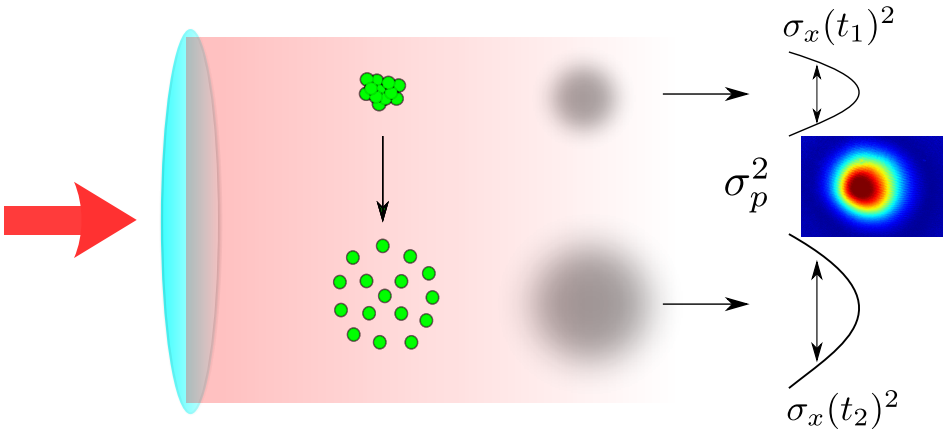

Figure 26 – The time of flight technique for two times of flight t_1 and t_2.
Source: By the author.

For a log enough expansion time (which is order of 10ms) we can assum that $\sigma_x(t_2) \gg \sigma_x(t_1)$. Then we can extract the temperature of the cloud with a single image through the expression:

$$T = \frac{m}{k_B}\left(\frac{\sigma_x(t_2)}{t}\right)^2 \tag{4.9}$$

Figure 26 shows the time of flight technique for cold atoms. The red arrow represents the image beam exerted on the atoms. The green balls represent the cloud of atoms expanding in z direction. The figure in gray color represent the shadow for each time of flight.

Figure 27 represents the time of flight technique for two dimensions, and was obtained by plotting the width of the cloud for each time in two dimensions but separately versus the time of flight between 10ms and 17ms.

To obtain the temperature T_x or T_y, we need to extract the slopes for each straight line represented by blue and red color respectively, them the slope is multiply by M the

mass of the atom and divided by k_B the Boltzmann constant, see (4.8).

Finally, the "real" temperature of our sample of atoms, is necessary to take the average between the two temperatures T_x and T_y.

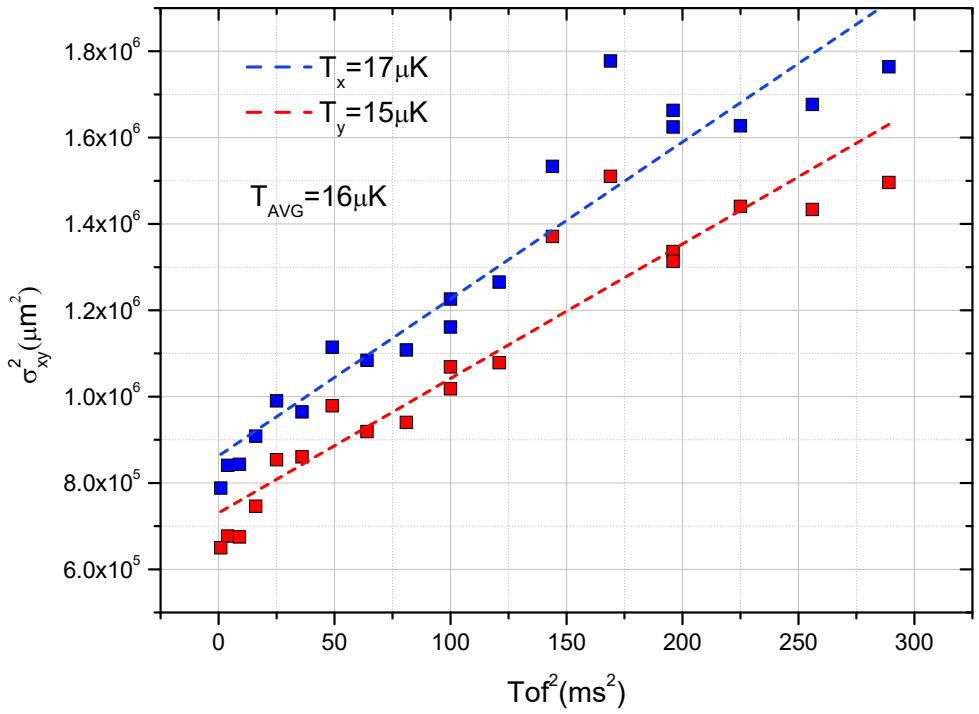

Figure 27 – The time of flight technique for different times of flight between 10ms and 17ms. The blue and red slope represent the temperature by fitting equation 5.6 for x and y dimension respectively.

Source: By the author.

To obtain the number of atoms, we need to introduce the optical density or optical depth $OD(x, y)$ and it could be expressed as $\sigma\rho_T(x, y)$, where the absorption cross section σ is given by:

$$\sigma = \frac{3\lambda^2}{2\pi}\frac{1}{1 + \frac{I}{I_s} + (\frac{2}{\Delta\Gamma})^2} \tag{4.10}$$

Where $\lambda = 770.108$nm, $I \ll I_s$, whose on-resoanance value is $\sigma = \sigma_0 = \frac{3\lambda^2}{2\pi}$.

$$OD(x, y) = OD_{peak} exp\left(-\frac{1}{2}\left[\frac{(x - x_0)^2}{\sigma_x^2} + \frac{(y - y_0)^2}{\sigma_y^2}\right]\right) \tag{4.11}$$

For a Gaussian atom density distribution (e.g. a distribution of non-interacting thermal atoms), the atom number N relates to the optical depth by:

$$N = \frac{1}{\sigma_0} \int OD(x, y) dx dy \tag{4.12}$$

Then, the number of atoms can be obtained from the integration of the equation (4.12):

$$N = \frac{2\pi}{\sigma_0} OD_{peak} \sigma_x \sigma_y \tag{4.13}$$

Where OD_{peak}, σ_x and σ_y are fit the values for a 2D Gaussian distribution describing the OD profile.

Finally, we can calculate the number of atoms in the Gray molasses stage. In this case, the optical density is $OD_{peak} = 1.30021$ and $\sigma_x \sigma_y = 1.4603 \times 10^6 \mu\text{m}^2$. Then, the number of atoms is $N = 4.2486 \times 10^7$ as typical obtained values.

5 RESULTS AND DISCUSSION

In this chapter, the experimental results concerning the ^{39}K (D1) Gray molasses will be presented. We investigate the influence of the relative detuning "d" between the two cooling frequencies and observe a decrease of the temperature and an increase in the number of atoms when the Raman condition is fulfilled. Furthermore, we investigate the influence of the global detuning "Δ" on the temperature. Finally, we present the final temperature as a function of the final D1 molasses power reaching the lowest temperature of 8.62μK. The optimization was done mainly by two criteria: to maximize the number of atoms and to minimize the temperature. The temperature of the cloud was obtained by the use of "Time of Flight Technique" see (4.8) and the number of atoms is calculated by the equation (4.13).

5.1 Characterization of Gray molasses

The final stage of cooling before transferring atoms into a magnetic trap is Gray molasses.

The capture velocity of this mechanism is quite low so it is useful to pre-cool the cloud to the lowest possible temperature. After the hybrid compress magneto optical trap stage, we turn off the magnetic field and the D2 light is replaced by the D1 light.

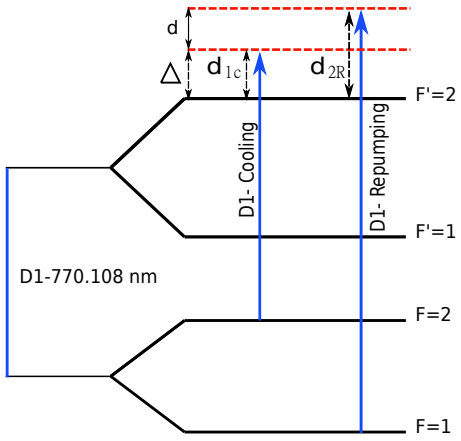

Figure 28 – Level scheme of the transitions used for D1 Gray molasses cooling for 39K working on the $F = 2 \rightarrow F' = 2$ transition.
Source: By the author.

5.1.1 Gray molasses timings

One further important parameter for Gray molasses are the timings, meaning the time between switching of the Hybrid-CMOT and applying the Gray molasses cooling.

We can optimize the temperature by scanning the duration of the Gray molasses as is shown in figure 29. This result shows us the behaviour of the temperature as a function of the duration of Gray molasses. We can observe that for a short period of time, the temperature show drops drastically from 300μK (Hybrid-CMOT) to 23μK approximately 1ms. This behaviour could be explained as follows: The lifetime of the transition is related to the inverse of the natural linewidth, that is, $1/\Gamma_{D1} \approx 26.37$ ns. Thus, in 1ms, the hole cloud experiences multiplies cycles of the Sysiphus cooling mechanism, being able to cold down the temperature in a short period of time. After this time, the diffusion of the cloud will increase, producing heating in this stage, since in Gray molasses there is not magnetic field.

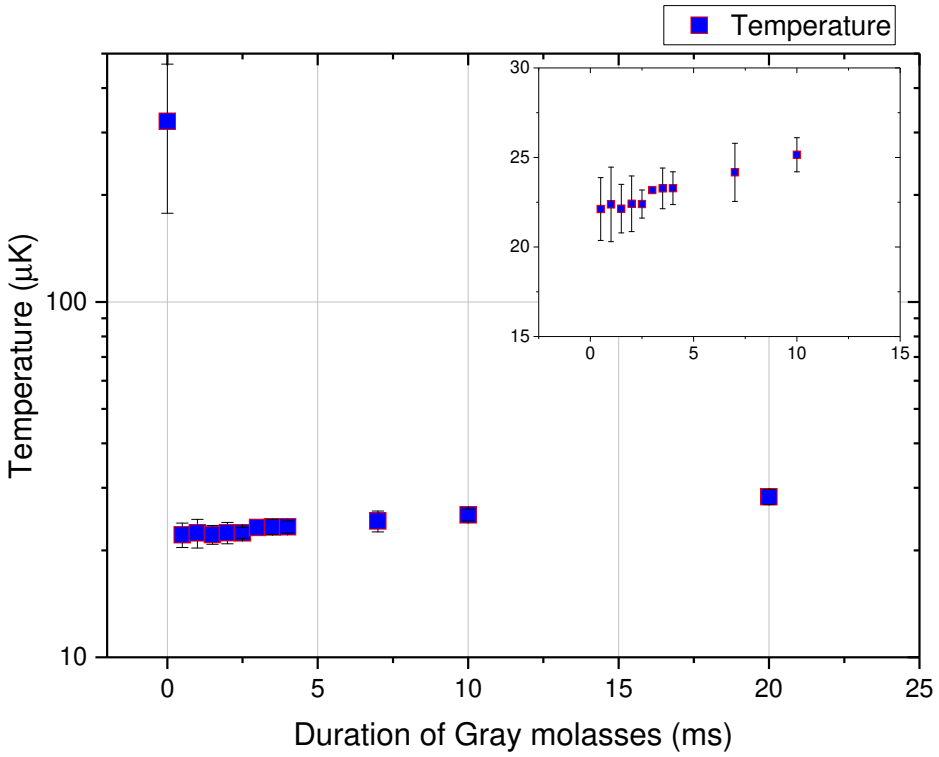

Figure 29 – Temperature as a function of duration in Gray molasses.
Source: By the author

Since our results are optimzed based on two criteria temperature and number of atoms. Therefore, figure 30 is a optimization of number of atoms as a function of the duration of Gray molasses. As we know, initially our sample has a temperature around 300 μK, for a long time of flight the cloud expand very fast, thus, we are limited to capture the hole cloud. How the temperature drops very fast, after 1ms, is possibel to us use the same time of flight in order to capture the hole cloud. Thus, after 1ms we can observe a constant number of atoms around 6×10^7. I would like to clarify that hat relative detuning was kept constant d but not optimized.

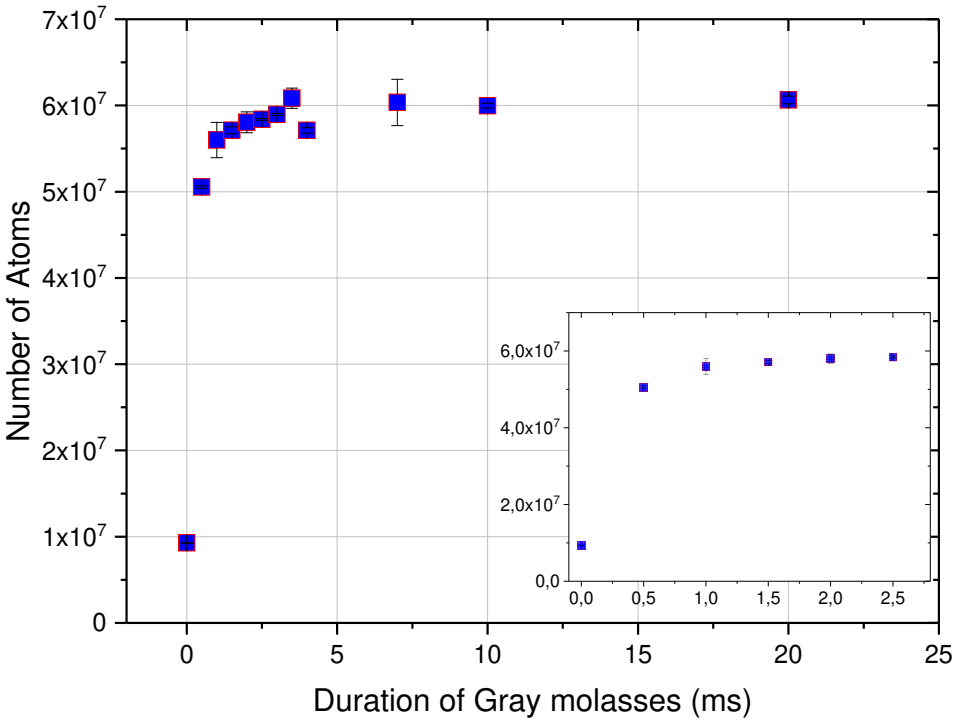

Figure 30 – Number of atoms as a function of duration in Gray molasses.
Source: By the author.

5.1.2 Raman detuning

We commence studying one of the most important steps to characterized Gray molasses, measuring the typical asymmetric Fano profile and its dependence with the temperature via the Raman detuning or relative detuning d. In this stage, Raman resonance condition must be fullfilled, in order to obtain the most efficient cooling. In other words, the relative detuning between the (D1) cooling and repumping lights, should be zero, that is $d = 0 = \delta_{1R} - \delta_{1C}$ as can be shown in 28. To perform this characterization, we set the

global detuning as $\Delta = 3.9\Gamma$ as a fixed value and equal to the detuning of the cooling light δ_{1C}, then the detuning of the repumper light works in a range between 3.84Γ and 3.93Γ, where $\Gamma = 2\pi \times 5.95$MHz being the decay rate of the (D1) line transition.

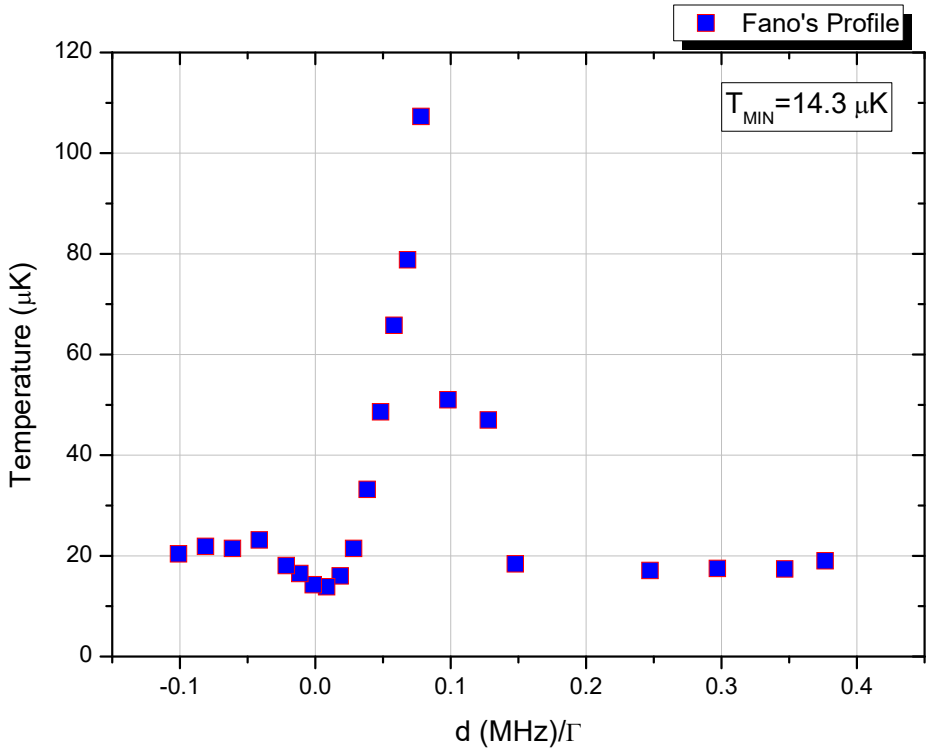

Figure 31 – Temperature of the (D1) Gray molasses as a function of Raman detuning d. Deep cooling is found at the Raman resonance. The cooling at 14.3 μK observed on both sides of the resonance is attributed to the Gray molasses mechanism working on the $F = 2 \rightarrow F' = 2$ transition.

Source: By the author.

As we can see in figure 31, the cooling is found to work best when the relative detuning is around $d \approx 0$ reaching temperatures around 14.3μK. Note that other parameters used in this measurement are fixed. Another important feature that we can see from figure 31 is that the relative detuning is not exactly $d = 0$, that could be interpreted as the result of the background magnetic fields after turn off the magnetic field, which shift the energy levels. If there is no detuning between the cooling and the repumper with respect to the excited level, additional Λ-systems emerge for the ground hyperfine manifolds and the result would be a lower temperature due to additional dark states on two photon resonance.

To the blue of the Raman resonance $\delta_{1R} > \delta_{1C}$, a heating peak is observed which

means at the case the atoms in dark states with more energy than that bright states and will gain kinetic energy when they motional coupled to bright states at the top of energy hills. This mechanism leads a strong heating, the temperature increases and tends to the Doppler temperature 140μK.

Whereas to the red of the Raman resonance $\delta_{1C} > \delta_{1R}$ has been showm thoerically and experimentall low temperatures over a certain range of negative values of d, a possible explanation is that occurs a weakly coupled states are formed due to coherence among the m_F sub-levels that belong to the same F level.

Another parameter that must be studied is the number of atoms as a function of relative detuning d as well, see figure 34. We find a maximum number of atoms 4×10^7 when the Raman condition is fullfilled. At the Raman resonance $d = 0$, atoms in dark states are maximally coupled to bright states at the bottom of energy hills, which induce a peak in the atom number. To the blue of the Raman resonance a significant loss of atom number during the molasses phase is observed, which is the inverse of Sisyphus cooling. This deep decay is due to the poor capture efficiency of the atoms, causing them to escape.

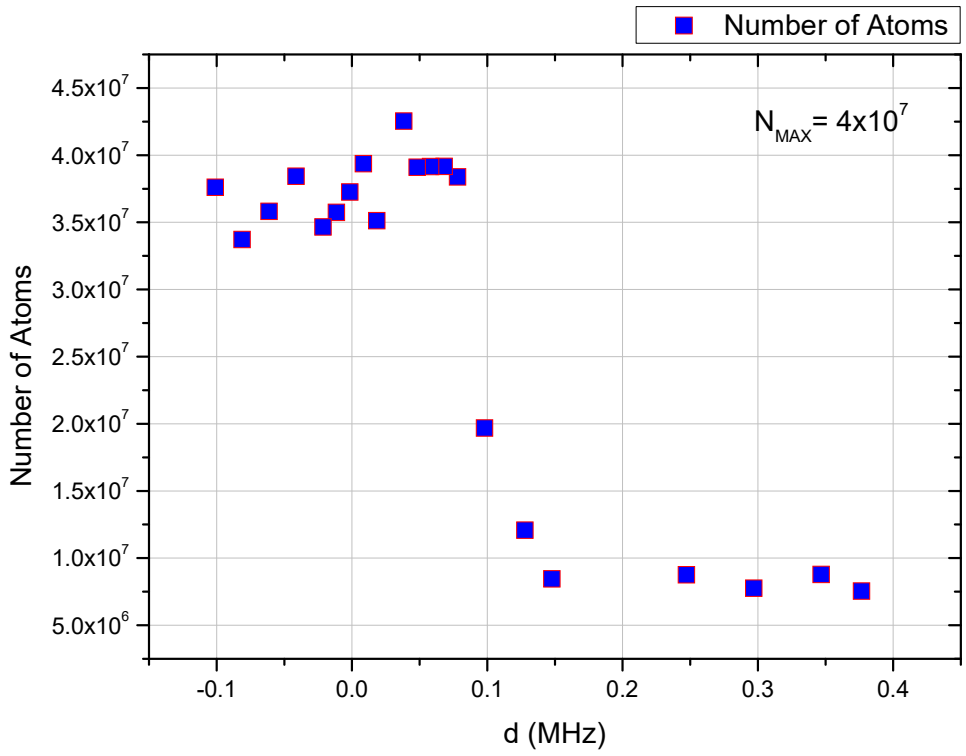

Figure 32 – Number of atoms in Gray molasses as a function of Raman detuning d.
Source: By the author.

In figure 33, we set the total power of the D1 light beam as $I = 8.5I_s$, and then, we study the temperature as a function of the global detuning $\Delta = \delta_{1C}$ of the D1 cooling beams in order to see, if the global detuning Δ has an influence on the temperature mantaining the Raman condition satisfied. The graph shows us that the temperature does not depend on this range of frequency 1Γ and 4.5Γ. To obtain this graph, the relative detuning d was kept constant for each δ_{1C} and δ_{1R} and showing us that the relative detuning is the only one that influences the temperature.

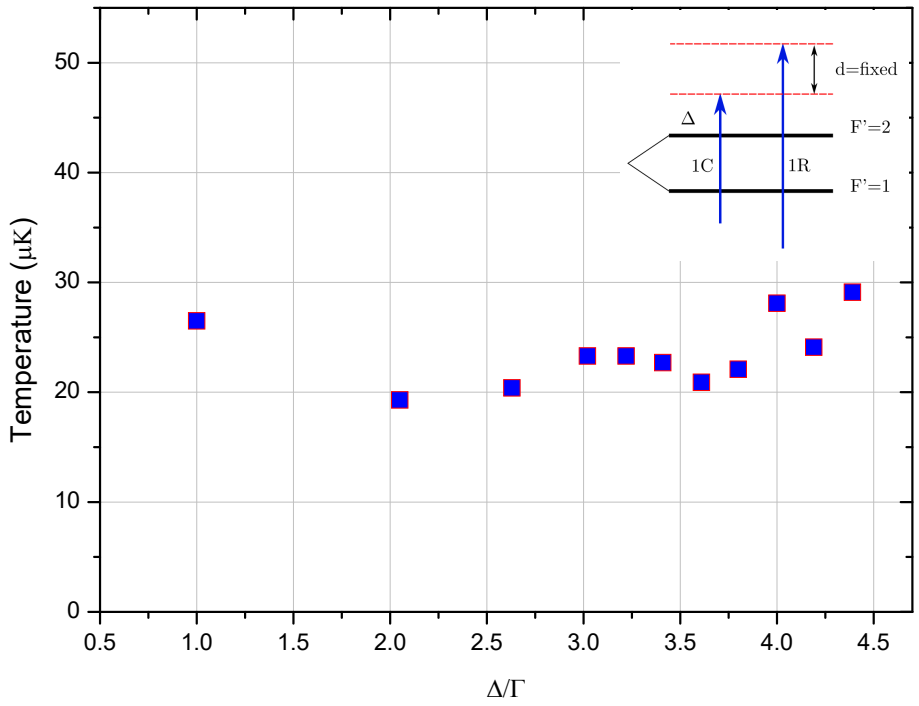

Figure 33 – Temperature of the (D1) gray molasses as a function of the global detuning Δ of the D1 cooling beams.

Source: By the author.

Our result shows similarity to that obtained by Salomon *et al.*[38] in this range of frequency. However, we were limited by the frequency tuning range of the double-passed AOM, thus the scan was performed between 1Γ and 4.5Γ above the $F' = 2$ state. Consequently, we cannot observe the behavior of temperature on resonance with the $F' = 2$ state, when the global detuning is $\Delta = 0$ and also we could not observe Gray molasses worikng with the $F' = 1$ state, contrary to what was reported in,[38] where a peak heating is observed -5Γ and for -7.5Γ a deep cooling is observed. It was interpreted as Gray molasses working with the $F' = 1$ state.

5.1.3 Light Intensity

In figure 35, we present the final temperature as a function of the total power (D1). We find the temperature decrease linearly with the final optical power. In this result, the detuning of the cooling is -37.5 MHz and the repumping is -17.14 MHz. This linear decrease may be understood, in analogy with the behavior of bright molasses according to $T = I/\Delta$, from the reduction of the induced light shifts in the dressed state picture. For an intensity $0.28I_s$, we find a minimal temperature of $(8.84 \pm 0.22)\mu$K reaching the lowest temperature in this dissertation. This graphic show us the importance of the power to dynamically tune the velocity capture range.

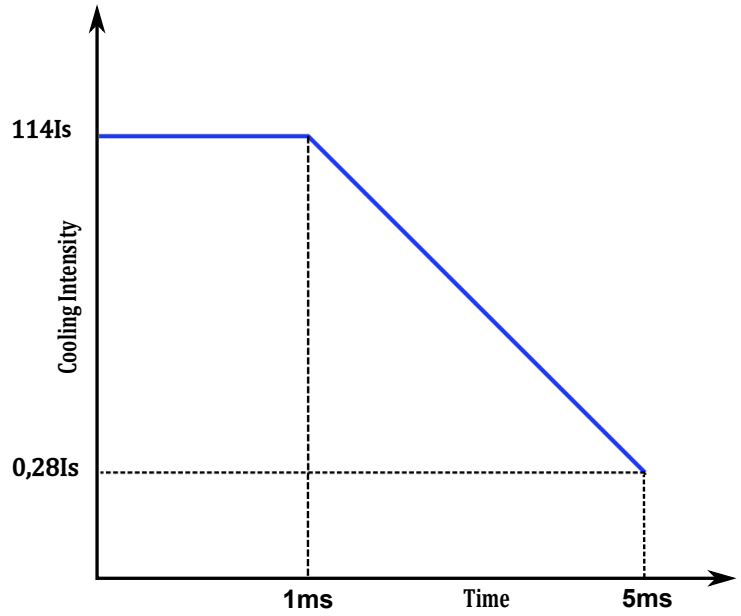

Figure 34 – Two-stage cooling scheme. A capture phase and constant cooling power at 114 I_s with a duration of 1 ms is followed by a cooling phase of 4ms in which the intensity is ramped down to 0.28 I_s of the initial cooling intensity.
Source: By the author.

In our laboratory, the cooling and the repumping beams are coupled to a single optical fiber. Then, the ratio between them was measured via Fabry Perrot whose signal is displayed as carrier and sidebands of the laser beam on a oscilloscope. The ratio of 4 : 1 of intensities of cooling and repumping. Consequently, we can not observe the behaviour of the temperature and the number of atoms in relation to each beam of light. Futhermore, we present an inset between (8.5 and 12)μK in order to see the minimum temperature obtained in the laboratory. If we start directly with this low intensity, the capture velocity of the Gray molasses is reduced.

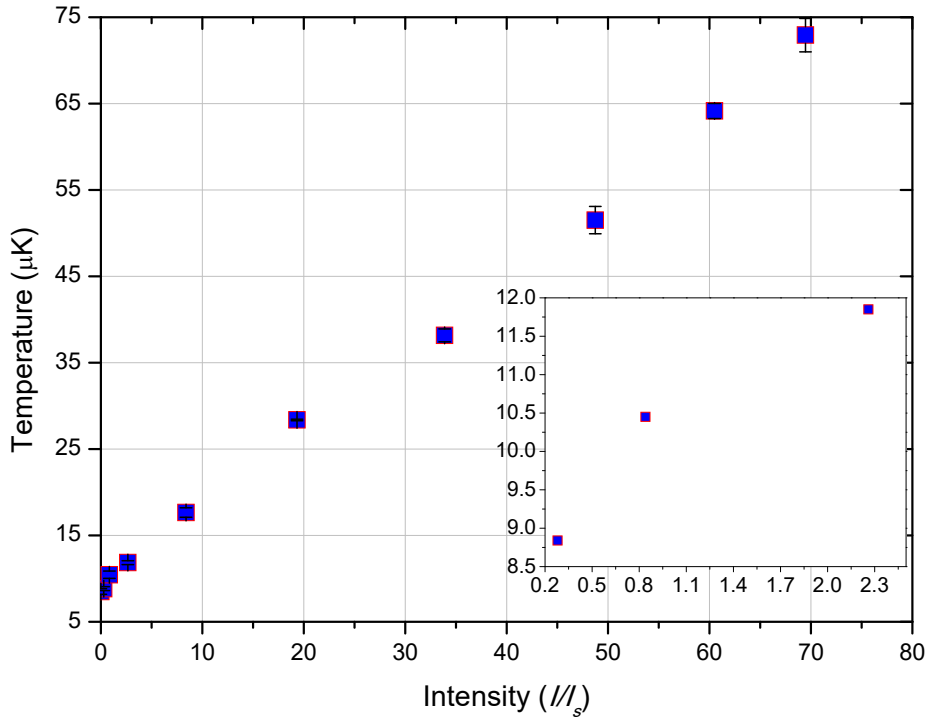

Figure 35 – Temperature of Gray molasses vs total power (D1) light beam.
Source: By the author.

5.2 Phase space density analisys

The phase space density or (PSD), is one of the most important property to analyze our atomic cloud and also it allow us to compare our results across different experiments. This property relates atomic density in real space in phase space.

To calculate the phase space density, we need to extract the peak density of the cloud by:

$$N = \int n_0 e^{\frac{-r^2}{2\sigma^2}} 4\pi r^2 dr = (2\pi)^{3/2} n_0 \sigma^3 \tag{5.1}$$

Where N is the total number of atoms in the cloud and σ is a width. From the image analysis we know N and σ.

$$n_0 = \frac{N}{(\pi/2)^{3/2}\sigma^3} \tag{5.2}$$

Finally, the phase space density at the center of the trap is given by:

$$\rho = \lambda_B^3 n_0 \tag{5.3}$$

Where $\lambda_B = \frac{h}{\sqrt{2\pi m k_B T}}$ is identified as the thermal de Broglie wavelength. For $\rho \ll 1$, the interparticle spacing is much larger than the size of the atomic wave packet and the gas can be described in the classical limit.

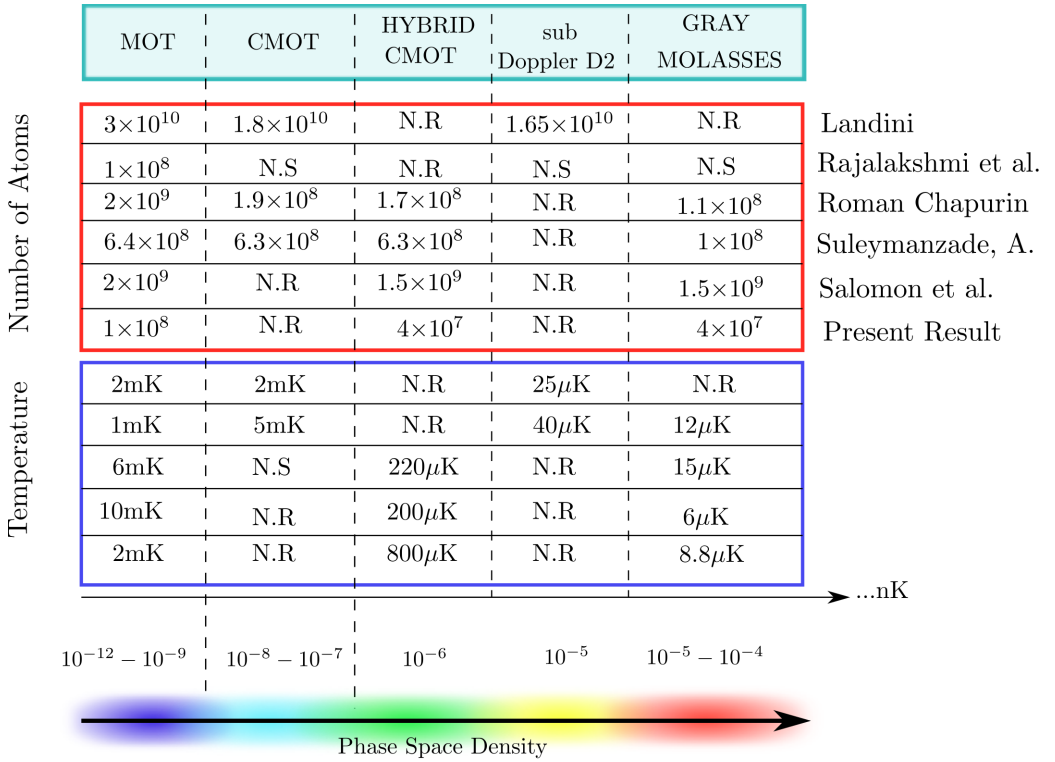

Figure 36 – Number of atoms, temperature and the phase space density fo some works related to precooling potassium atoms. NR: Not realized, NS: Not specified.
Source: By the author.

Figure 36, show us the main parameters such as the number of atoms, temperature and the phase space density for each pre-cooling stages, during the Magneto Optical Trap MOT, Compressed MOT, Hybrid CMOT D1-D2, sub Doppler cooling using the D2 line and Gray molasses reported by some theses and scientific publications.

We can notice that the number of atoms during different pre-cooling stages is almost constant. However, the parameter that is most affected for each stage is the temperature. It goes from mK to μK.

At the bottom of the figure as expected the phase space density increases from left to right as the temperature decreases at each stage, following the equation (5.3).

At the begining of the sequence, we can see that our magneto optical trap starts

with a low number of atoms compared to other experiments, and later we lose an order of magnitud during the Hybrid CMOT stage. Despite the fact that we managed to reduce the temperature, this being compatible with other reported results, Although we managed to reduce the temperature, being compatible with other reported results, our phase space density is the lowest due to the low number of atoms.

6 CONCLUSIONS AND PROSPECTS

As mentioned before, our laboratory has a research focus on the obtention and studies of a two-component BEC. The chosen species are Na and K. By an issue of abundance, we have decided to move to 39K and implement the technique. Its implementation, characterization and studies are the main objectives of this dissertation. In this work, we have presented an extensive literature revision, as well as, we have made a detailed description of the experimental apparatus of our system. In this context, we have obtained the lowest temperature on a thermal cloud ever obtained in our lab, something around 8 micro K. This achievement was possible by scanning and optimizing different parameters concern Gray Molasses techniques. It is very important for the next steps of the time sequence to the two-component BEC. We have found that our cloud preparation leads us to something very compatible in therm of temperatures comparing to other laboratory results. In terms of the number of atoms, we have found that our values are a little below comparing other labs. This parameter is very important to consider, and we have some strategies to improve this aspect, and we will intend to implement them soon. Among those strategies is the revision of the 2D MOT for potassium. Attached to 2D MOT, is the Zeeman slower that also can be improved in terms of adjustments in the magnetic field and frequency. Anyway, we can conclude we have reached our main objective of obtaining the lowest temperature possible under the condition we have at this moment. Also, we have made a study comparing the phase space density we have to ones from other labs and confirm our issue is the number of atoms that we will work on soon.

REFERENCES

1 BOSE. Plancks Gesetz und Lichtquantenhypothese. **Zeitschrift für Physik**, v. 26, p. 178–181, 1924. DOI:10.1007/BF01327326.

2 EINSTEIN, A. Quantentheorie des einatomigen idealen gases. zweite abhandlung.ng. *In:* SIMON, D. (ed.). **Albert Einstein:** akademie-vorträge. New York: John Wiley & Sons, Ltd,2006. p.245-257. DOI:10.1002/3527608958.ch28.

3 RASTOGI, A. **Light-matter interactions for quantum simulation and quantum memory experiments**. 2018. Dissertation (Master of Science) — Department of Physics, University of Alberta, Edmonto, 2018.

4 KAPUSTA, J. I. Bose-Einstein condensation, spontaneous symmetry breaking, and gauge theories. **Physical Review D**, American Physical Society, v. 24, p. 426–439, July 1981. DOI:10.1103/PhysRevD.24.426.

5 MEWES, M.-O. *et al.* Output coupler for Bose-Einstein condensed atoms. **Physical Review Letters**, v. 78, n. 4, p. 582–585, Jan. 1997.

6 MADISON, K. W. *et al.* Vortex formation in a stirred Bose-Einstein condensate. **Physical Review Letters.**, American Physical Society, v. 84, p. 806–809, Jan. 2000. DOI:10.1103/PhysRevLett.84.806.

7 BILLY, J. *et al.* Direct observation of anderson localization of matter waves in a controlled disorder. **Nature**, Springer Science and Business Media LLC, v. 453, n. 7197, p. 891–894, June 2008. DOI:10.1038/nature07000.

8 ROATI, G. *et al.* Anderson localization of a non-interacting Bose–Einstein condensate. **Nature**, v. 453, n. 7197, p. 895–898, 2008.

9 BLOCH, I.; DALIBARD, J.; ZWERGER, W. Many-body physics with ultracold gases. **Reviews of Modern Physics**, v. 80, n. 3, p. 885–964, 2008.

10 GREINER, M. *et al.* Quantum phase transition from a superfluid to a mott insulator in a gas of ultracold atoms. **Nature**, v. 415, n. 6867, p. 39–44, 2002.

11 HENN, E. A. L. *et al.* Bose-Einstein Condensation in 87Rb: characterization of the Brazilian Experiment. **Brazilian Journal of Physics**, v. 38, n. 2, p. 279–286, June 2008.

12 TAVARES, P. *et al.* Out-of-phase oscillation between superfluid and thermal components for a trapped Bose condensate under oscillatory excitation. **Laser Physics Letters**, v. 10, n. 4, p. 045501, 2013.

13 HENN, E. A. L. *et al.* Observation of vortex formation in an oscillating trapped Bose-Einstein condensate. **Physical Review A**, v. 79, n. 4, p. 043618, 2009. DOI:10.1103/PhysRevA.79.043618.

14 HENN, E. A. L. *et al.* Emergence of turbulence in an oscillating Bose-Einstein condensate. **Physical Review Letters**, American Physical Society, v. 103, n. 4, p. 045301, July 2009. DOI:10.1103/PhysRevLett.103.045301.

15 CATANI, J. *et al.* Intense slow beams of bosonic potassium isotopes. **Physical Review A**, American Physical Society, v. 73, n. 3, p. 033415, Mar. 2006. DOI:10.1103/PhysRevA.73.033415.

16 LAMPORESI, G. *et al.* Compact high-flux source of cold sodium atoms. **Review of Scientific Instruments**, v. 84 6, n. 6, p. 063102, 2013.

17 SCHULZE, T. A. **Quantum degenerate mixtures of 23Na-39K and coherent transfer paths in NaK molecules**. 2018. Ph. D. Thesis (Doctor) — Hannover: Institutionelles Repositorium der Leibniz, Universität Hannover, Hannover, 2018.

18 SHAHRIAR, M. S. *et al.* Continuous polarization-gradient precooling-assisted velocity-selective coherent population trapping. **Physical Review A**, American Physical Society, v. 48, p. R4035–R4038, Dec. 1993. DOI:10.1103/PhysRevA.48.R4035.

19 WEIDEMÜLLER, M. *et al.* A novel scheme for efficient cooling below the photon recoil limit. **EPL (**Europhysics Letters), v. 27, n. 2, p. 109, 2007.

20 BOIRON, D. *et al.* Three-dimensional cooling of cesium atoms in four-beam gray optical molasses. **Physical Review A**, American Physical Society, v. 52, p. R3425–R3428, Nov. 1995. DOI:10.1103/PhysRevA.52.R3425.

21 BOIRON, D. *et al.* Laser cooling of cesium atoms in gray optical molasses down to 1.1 μk. **Physical Review A**, American Physical Society, v. 53, n. 6, p. R3734–R3737, June 1996. DOI: 10.1103/PhysRevA.53.R3734.

22 ESSLINGER, T. *et al.* Purely optical dark lattice. **Optics Letters**, OSA, v. 21, n. 13, p. 991–993, July 1996.

23 BRUCE, G. D. *et al.* Sub-doppler laser cooling of40k with raman gray molasses on the D_2 line. **Journal of Physics B:** atomic, molecular and optical physics, IOP Publishing, v. 50, n. 9, p. 095002, Apr. 2017. DOI:10.1088/1361-6455/aa65ea.

24 ROSI, S. *et al.* -enhanced grey molasses on the d2 transition of rubidium-87 atoms. **Scientific Reports**, v. 8, p. 1301, 2018. DOI:10.1038/s41598-018-19814-z.

25 SHI, Z. *et al.* Sub-doppler laser cooling of {23}na in gray molasses on the d{2} line. **Chinese Physics Letters**, v. 35, n. 12, p. 123701, 2018.

26 COOK, R. J. Atomic motion in resonant radiation: an application of ehrenfest's theorem. **Physical Review A**, APS, v. 20, n. 1, p. 224, 1979.

27 HÄNSCH, T. W.; SCHAWLOW, A. L. Cooling of gases by laser radiation. **Optics Communications**, Elsevier, v. 13, n. 1, p. 68–69, 1975.

28 TAMMUZ, N. **Thermodynamics of ultracold 39K atomic Bose gases with tuneable interactions**. 2012. Ph. D. Thesis (Doctor) — University of Cambridge, Cambridge, 2012.

29 LETT, P. D. *et al.* Optical molasses. **JOSA B**, Optical Society of America, v. 6, n. 11, p. 2084–2107, 1989.

30 ADAMS, C. S.; RIIS, E. Laser cooling and manipulation of neutral particles. **The New Optics**, p. 1–39, 1997.

31 MARUYAMA, R. **Optical trapping of ytterbium atoms**. 2003. Ph. D. Thesis (Doctor) — University of Washington, Washington, 2003.

32 DALIBARD, J.; COHEN-TANNOUDJI, C. Laser cooling below the doppler limit by polarization gradients: simple theoretical models. **Journal of the Optical Society of America B**, Optical Society of America, v. 6, n. 11, p. 2023–2045, 1989.

33 COHEN-TANNOUDJI, C. Atomic motion in laser light. *In:* RAIMOND, J.-M.; ZINN-JUSTIN, J. (ed.). **Fundamental systems in quantum optics.** Amsterdam: North Holland, 1990. p. 1-164. (Les Houches, n.53).

34 HOPKINS, S. A. **Laser cooling of rubidium atoms in a magneto-optical trap**. 1996. Ph. D. Thesis (Doctor) — The Open University, Milton Keynes, 1996.

35 TIECKE, T. **Properties of potassium**. 2010. Ph. D. Thesis (Doctor) — University of Amsterdam, The Netherlands, 2010.

36 SHAHRIAR, M. *et al.* Continuous polarization-gradient precooling-assisted velocity-selective coherent population trapping. **Physical Review A**, APS, v. 48, n. 6, p. R4035, 1993.

37 WEIDEMÜLLER, M. *et al.* A novel scheme for efficient cooling below the photon recoil limit. **EPL (Europhysics Letters)**, IOP Publishing, v. 27, n. 2, p. 109, 1994.

38 SALOMON, G. *et al.* Gray-molasses cooling of 39k to a high phase-space density. **EPL (Europhysics Letters)**, IOP Publishing, v. 104, n. 6, p. 63002, 2014.

39 FERNANDES, D. R. *et al.* Sub-doppler laser cooling of fermionic 40k atoms in three-dimensional gray optical molasses. **EPL (Europhysics Letters)**, IOP Publishing, v. 100, n. 6, p. 63001, 2012.

40 CHEN, H.-Z. *et al.* Production of large k 41 bose-einstein condensates using d 1 gray molasses. **Physical Review A**, APS, v. 94, n. 3, p. 033408, 2016.

41 COLZI, G. *et al.* Sub-doppler cooling of sodium atoms in gray molasses. **Physical Review A**, APS, v. 93, n. 2, p. 023421, 2016.

42 ASPECT, A. *et al.* Laser cooling below the one-photon recoil energy by velocity-selective coherent population trapping. **Physical Review Letters**, APS, v. 61, n. 7, p. 826, 1988.

43 ASPECT, A. *et al.* Laser cooling below the one-photon recoil energy by velocity-selective coherent population trapping: theoretical analysis. **Journal of the Optical Society of America B.**, Optical Society of America, v. 6, n. 11, p. 2112–2124, 1989.

44 CASTIN, Y.; DALIBARD, J.; COHEN-TANNOUDJI, C. **The limits of sisyphus cooling.** 1991. Availbale from: http://pro.collegedefrance.fr/jean.dalibard/publications/Elba1990.pdf. Accessible at: 23 Jan. 2021.

45 METCALF, P. v. d. S. H. J. **Laser cooling and trapping**. Berlin: Springer, 1999. (Graduate texts in contemporary physics).

46 PAPOFF, F.; MAURI, F.; ARIMONDO, E. Transient velocity-selective coherent population trapping in one dimension. **Journal of the Optical Society of America B.**, Optical Society of America, v. 9, n. 3, p. 321–331, 1992.

47 SHAMMOUT, B. **A laser system for Gray-Molasses cooling on the D1 Transition of an Atomic Gas of 39K**. 2020. Dissertation (Master of Science) — Institut fur Quantenoptik, Leibniz Universitat Hannover, 2020.

48 CASTILHO, P. *et al.* A compact experimental machine for studying tunable bose–bose superfluid mixtures. **Laser Physics Letters**, IOP Publishing, v. 16, n. 3, p. 035501, 2019.

49 PEÑAFIEL, E. E. P. **Production of a Bose-Einstein condensate of sodium atoms and investigation considering non-linear atom-photon interactions**. 2016. Ph. D. (Doctor of Science) — Instituto de Física de São Carlos, Universidade de São Paulo, São Carlos, 2016.

50 CASTILHO, P. C. M. **New experimental system to study coupled vortices in a two-species Bose-Einstein condensate 23Na-41K with tunable interactions**. 2017. Ph. D. Thesis (Doctor of Science)— Instituto de Física de São Carlos, Universidade de São Paulo, São Carlos, 2017.

51 MCKAY, D. *et al.* Low-temperature high-density magneto-optical trapping of potassium using the open 4 s→ 5 p transition at 405 nm. **Physical Review A**, APS, v. 84, n. 6, p. 063420, 2011.

52 KETTERLE, W.; DURFEE, D. S.; STAMPER-KURN, D. **Making, probing and understanding Bose-Einstein condensates**. 1999. Available from:https://arxiv.org/pdf/cond-mat/9904034.pdf. Accessible at: 23 Jan. 2021.

53 MAZO, P. L. **Controlling the interaction via Feshbach resonances in a dual-species Bose-Einstein condensate:** the implementation for potassium. 2020. Dissertation (Master of Science) — Instituto de Física de São Carlos, Universidade de São Paulo, São Carlos, 2020.